Wesleyan University

A Search for Hα Absorption of the Extended Atmosphere of TOI-1288b, a Giant Planet in the Neptune Desert

by

Lisseth Gonzales Quevedo
Class of 2024

A thesis submitted to the
faculty of Wesleyan University
in partial fulfillment of the requirements for the
Degree of Master of Arts

Middletown, Connecticut
May, 2024

In one of the stars I shall be living. In one of them I shall be laughing. And so it will be as if all the stars were laughing, when you look at the sky at night . . . You — only you — will have stars that can laugh!

—Antoine de Saint-Exupéry

The Little Prince

Acknowledgements

Achieving something in life is not easy work, and it is not a solo journey. Throughout our lives, we have people who help us grow and become better versions of ourselves. During my time at Wesleyan, I have met amazing people who have directly or indirectly contributed to this moment in my life and whom I would like to thank from the bottom of my heart.

Words cannot express my deepest gratitude and appreciation to my advisor, Seth Redfield. This endeavor would not have been possible without your guidance, patience, and unconditional support. Thank you very much for believing in me. Even when I thought I would not make it, you always encouraged me to continue and not give up. And as it says in my country, "¡Vales un Perú!". Also, I would like to extend my gratitude to Professors Meredith Hughes, Sarah Wellons, Ed Moran, and Roy Kilgard. Thank you all for your teaching and support and for making the department feel like a family.

The Wesleyan Astronomy Department would not be what it is if it were not for the community that makes it up, between postdocs, masters students, undergraduate students, and staff. I would like to thank post-docs Jonathan Jackson, Azmain Nisak, and Brianna Zawadzki for their support and friendship. I express my gratitude to Sara Nagussi and Alaina Einsig for all the shared moments of learning and leisure during my first year. In the same line, my thanks and gratitude also go to Catherine Sarosi and Katie Ciurleo. Thank you for showing me the meaning of friendship. My special thanks, appreciation, and gratitude to my co-worker, friend, and family by choice, Rewa Bush. I feel fortunate to have you in my life.

I want to express my gratitude and sincere thanks to Stefanie Dinneen for con-

stantly checking on me and for being a fantastic person. I also want to thank my undergrad partners Carlos Ordoñez (my foosball friend), Chris Tian, Owen Gonzales, Aliya Nurmohamed, Jamar Kittling, Caroline Lamoureux, Elias Mansell, Kyle McGregor, Matteo Andres, Sofia Rinaldi, Junu Lee, Dylan McCaleb, and Uday Narayanan. Thanks all for being part of this stage of my life.

I would like to thank Cheryl-Ann Hagne and Barbara Schukoske for their help, especially in difficult times. Many thanks to my friends Max Hanrahan and Samitha Salkuja and especially to my dear friend and family by choice, Pritha Sengupta; thanks for being an amazing person and being there for me in my hard moments.

I want to express my gratitude to my academic family in Peru; I would not have gotten here without them. To my professors, Teófilo Vargas and Víctor Vera, for their encouragement to always follow my goals. Also, I express my special gratitude and appreciation to my research advisor, Daniella Bardalez Bagliuffi, for her advice and guidance on my path to reaching the stars.

I reserved this paragraph for my loving and amazing parents, Javier and Cecilia. I could not have dreamed of better parents than you. Thanks to you for your constant support and encouragement and for teaching me that there are no limits if you work for your dreams. To my dear brothers Max and Xavier and my little sister Nathalie, thanks for always being there for me. I love you guys and will forever be grateful for your presence in my life!!!

Gracias totales a todos y cada uno de ustedes quienes han hecho que mi paso por Wesleyan sea una de las mejores experiencias en vida, la cual siempre llevaré en el corazón.

Contents

Chapter 1

Introduction

1.1 Worlds Beyond Our Solar System

1.1.1 What is an exoplanet?

Since the beginning of human history, there have been voices about the existence of other worlds beyond the borders of our Solar System. In 341–270 B.C.E, the Greek philosopher Epicurus, in a letter to Herodotus, made an argument: "There is an infinite number of worlds, some like this world, others unlike it". Following the same line, but many years later, in 1584 the Italian philosopher Giordano Bruno published De l'infinito universo et mondi (On the Infinite Universe and Worlds), where he said the following: "There are therefore innumerable suns; there are infinite earths that equally revolve around these suns, in the same way as we see these seven (planets) revolve around this sun that is close to us" (Bruno 1980).

Unfortunately, that and other revolutionary ideas of Bruno were not very well regarded at that time, resulting in his imprisonment and execution as a heretic. However, nowadays talking about exoplanets is nothing new, and every year we see new candidates and confirmed discoveries of exoplanets.

Paice & J. C Watkins (2022) suggested that the rate of exoplanet discovery doubles roughly every 39 months, and that shows an interesting increase in the

number of exoplanets in our galaxy. This huge rate of discovery of exoplanets orbiting different stars than our Sun has had a huge impact in the last three decades. So, from just the idea about the existence of these worlds so far we have 5,523 exoplanets confirmed by the NASA Exoplanet Archive[1].

Exoplanetary sciences seem to have a promising future due to missions such as the *James Webb telescope (JWST)*, which will help the astronomy community in the path to answer questions such as "How do the planets evolve"?, and "Is there life on other planets?". Answering those questions will allow us to understand the evolution of planets like Earth and also any other needed parameters for finding life in a different planetary system. Due to the range of implications that exoplanet science has, it is not just an interest of the astronomy community. In fact, it works as a partner with other sciences such as biology.

1.1.2   The first confirmed signals of exoplanet detection

In 1992, the first exoplanet detection was confirmed. That extraordinary discovery was also a surprise because the discovered exoplanet was not orbiting a solar-type or mains sequence star. Wolszczan & Frail (1992) discovered a planetary system of two exoplanets orbiting a pulsar PSR1257+12. They found that the millisecond timing variation in this rapidly rotating neutron star was not due to a stellar companion but to two or more exoplanets. The planets around a pulsar were explained to be "second generation" planets, which means they were formed after the pulsar's evolutionary history. That suggestion opened a window for more questions in the astronomical community and scientist in general about their understanding of stellar and planetary evolution.

---

[1]https://exoplanetarchive.ipac.caltech.edu/.

A couple of years later, a new planetary system was discovered. Mayor & Queloz (1995) found a $0.5 M_J$ planet orbiting a solar-type star 51 Pegasi. 51 Pegasi b, as it was named, was discovered using the radial velocity technique (a technique that observes the Doppler shift of a star as it orbits the common center of mass of the system) at 0.05 AU and with an orbital period of 4.23 days. The proximity of 51 Pegasi b, compared to the planets in our solar system, is located within the orbit of Mercury. This was a surprise because a gas-giant planet was not expected to be found near its host star, which opened a new frontier to understanding the formation of giant planets. Thus began the study of "hot Jupiters.

The radial velocity technique dominated exoplanet detection for the next few years. However, in 2000, two independent research groups Henry et al. (2000) and Charbonneau et al. (2000) observed an exoplanet (HD-209458b) passing across the front of the star HD-209458. That was the first time that the transit method was used to confirm a radial velocity detection.

The transit method occurs when a planet or any object passes in front of a star, causing its brightness (stellar flux) to decrease slightly, as shown in Figure 1.1. We can observe this phenomenon in our solar system when Mercury and Venus occasionally pass across the front of the Sun. Introducing the transit photometry method in exoplanet detections and combining it with the radial velocity measurements provides to estimate the planet's radius and in addition, constrains its mass, surface gravity, and average density (Charbonneau et al. 2000).

The flux reduction of the star seen from the Earth is related to the size of the planet that is crossing in front of it. Using the transit method, we can determine the radius of the exoplanet, and a simple way to do this is if the star's appearance can be modeled as a circle with uniform brightness. Then the ratio of the planetary radius (R_{planet}) and stellar radius ($R_\star$) can be estimated from the transit depth δ

(Heller 2019).

$$\delta = \left(\frac{R_{Planet}}{R_\star}\right)^2 \tag{1.1}$$
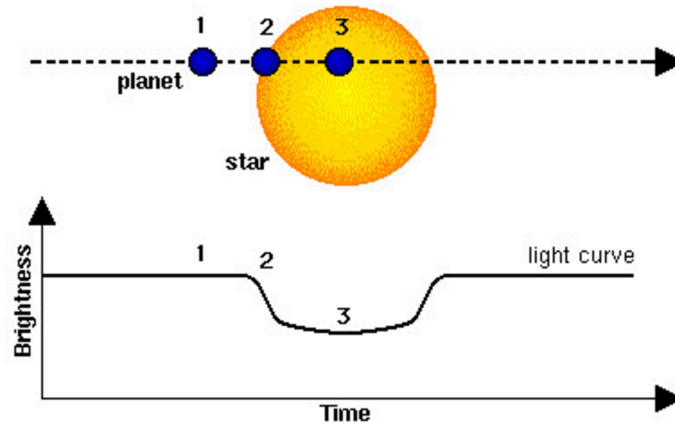

Figure 1.1: The transit technique shows how the star's brightness reduces when a planet is transiting in front of it. Image courtesy of ESA.

We can notice from Figure 1.1 that $R_{planet} << R_\star$, which means that $\delta << 1$. Therefore, from the exoplanet detection using the transit method, astronomers have observed that giant planets orbiting a solar-type star cause a transit depth of 0.01, while the transit depth for small rocky planets is approximately 0.0001. Because of this, gas giant planets with short periods are easy to find and characterize. These observational biases also add that the system must be aligned close edge-on to detect a transit.

1.1.3   The current era of exoplanets

Following the exoplanet detection timeline, we can see how it has developed since the first detection in 1992. At the current time, there have been found 5572 exoplanets. Figure 1.2 shows the current accumulative exoplanet detection per

year for the different detection methods. We can see that to date the transit method is one of the most successful methods in detecting exoplanets. However, at the end of 1995, there were only five known exoplanets (Three discovered by pulsar timing and two from radial velocities). From 1996 to 2013, the amount of discovered exoplanets was dominated by the radial velocity method, but since 2018, 78% had been discovered by the transit method (Deeg & Alonso 2018).
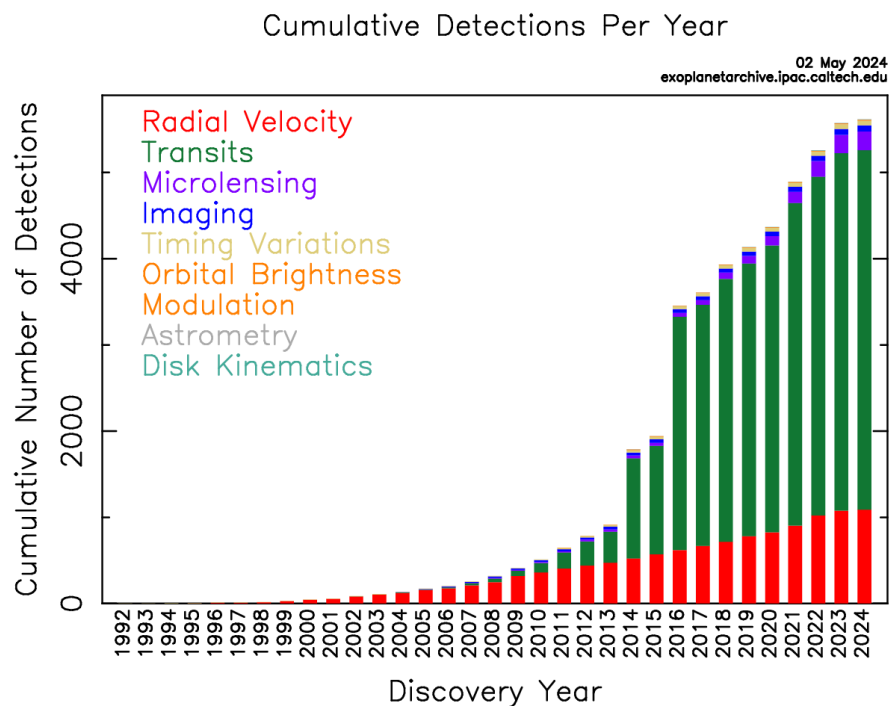
Figure 1.2: Cumulative exoplanet detection per discovery year by detection methods. Since the first discovered exoplanet the number of detections has grown exponentially, where most of them have been detected using the transit and radial velocity method. Image courtesy of NASA Exoplanet Archive.

One of the main reasons for improving exoplanet detection is intrinsically related to ground-based and space telescopes. *CoRoT (Convection, Rotation, and Transits)* was the first space mission dedicated to exoplanets. This space telescope was launched in December 2006 by the French space agency CNES. In 2009 the *Kepler* space telescope was launched, this telescope was NASA's first planet-

hunting mission. It observed the same portion of the Milky Way for 4 years to search for Earth-sized planets. Due to a failure in the spacecraft's reaction wheels, Kepler ended its operations in 2013. However, in 2014, *Kepler* returned its observation under the *K2* name. This new extended mission of *K2* ended in 2018 when the spacecraft ran out of fuel.

In April 2018, the *Transiting Exoplanets Survey Satellite (TESS)* was launched by NASA, and unlike *Kepler*, *TESS* scanned more than 85% of the entire sky to search for planets transiting bright and nearby stars. Stars near the ecliptic poles will have the longest observing intervals, being optimal locations for follow-up observations with the *JWST* (Ricker et al. 2015). The *JWST* is built in collaboration between NASA, the European Space Agency (ESA), and the Canadian Space Agency. This infrared observatory was launched in 2021 to investigate the galaxy's first light in the early universe, stars' birth, evolution of the solar system, and planets orbiting other stars (Menzel et al. 2023).

In contrast, there are ground-based telescopes such as *HAT (Hungarian-made Automated Telescope)* which cover two hemispheres. *HATnet*, active since 2003 and has been located at Mauna Kea Observatory (Hawaii), and *HATSouth* has been located at Las Campanas Observatory (Chile) since 2009 (Deeg & Alonso 2018). *WASP(Wide Angle Search for Planets)*, also covered two hemispheres, with *SuperWASP-North* located at Roque de los Muchachos Observatory on the Canary Island of La Palma (Spain) since 2004, and *WASP-South*, since 2006 at the South African Astronomical Observatory. The *Next-Generation Transit Survey (NGTS)* has been located at ESO's Paranal Observatory (Chile) since 2016.

So, between space telescopes and ground-based telescopes (here we mentioned just a few of them) and current scientific development, astronomers have been able to find a significant number of worlds beyond our solar system. However,

Figure 1.3 shows the mass-period distribution of discovered exoplanets, where we can observe critical biases for each detection method. In the case of the radial velocity and the transit method, we see that both methods are biased for large planets with short periods; therefore, that can explain why the current science has been focused on the study of hot Jupiters while Neptune-size planets, which are located in the "Neptune desert" (Section 1.3.1) are not well known.
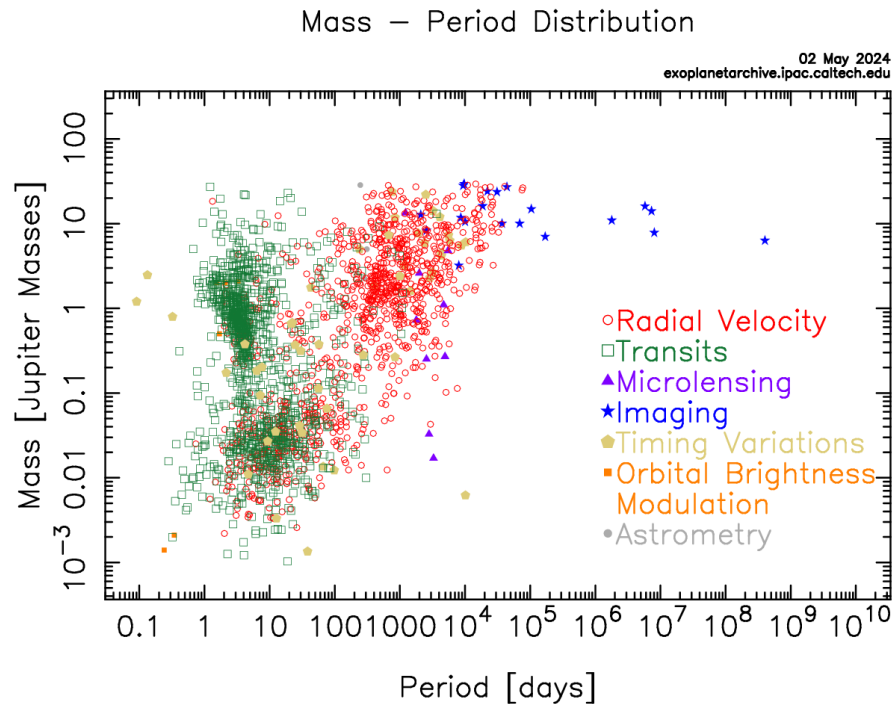
Figure 1.3: Mass ratio and period of exoplanets by detection method. This image shows that most detections have been made for short periods of high-mass exoplanets. It is also notable that the transit method is more sensitive to lower-mass planets compared with the radial velocity method. Image courtesy of NASA Exoplanet Archive.

1.2 Transmission spectrum and the exoplanet atmosphere characterization

Considering the time we have been studying the skies and objects like stars, it seems that our knowledge about exoplanets has just begun. However, astronomers

have developed methods that can help us study these distant worlds. As mentioned in the previous section, radial velocity and transit methods can provide important information about them.

The radial velocity method gives a planet's mass, and the transit method provides the exoplanet's radius. So, the complement of these two techniques provides relevant features that allow us to characterize them. However, if we want to know the exoplanet's atmosphere composition, we need to approach the problem differently using a method called transmission spectroscopy.

The transmission spectroscopy method measures the planet's apparent change in size as a function of wavelength, where the light from the host star passes through the planet's atmospheric annulus to interact with atoms and molecules. So, an opaque annulus is observed due to the strong absorption at specific wavelengths of chemical species in the planetary atmosphere (Mayorga et al. 2021).
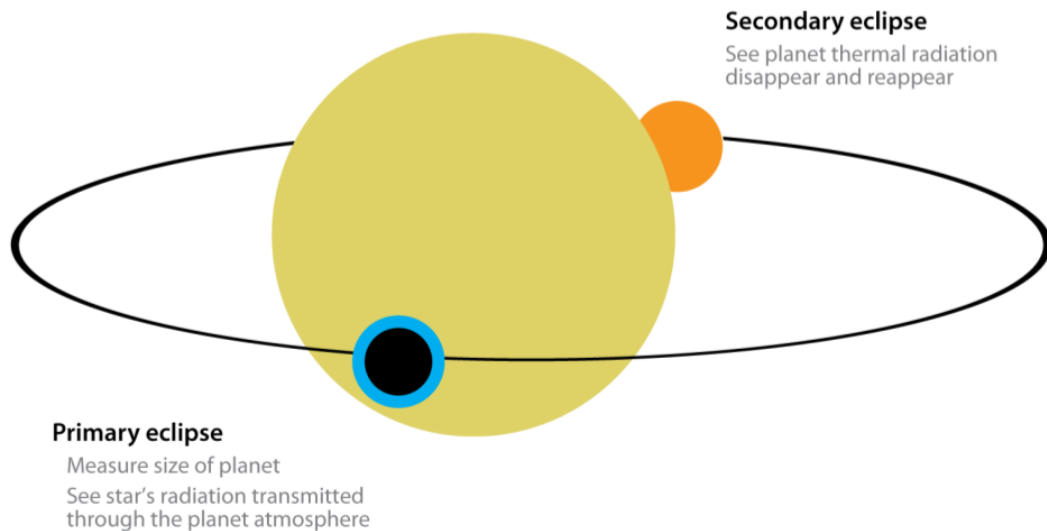

Figure 1.4: schema of a planetary transit, where the planet transits in front of its host star, and a portion of the starlight passes through the planetary atmosphere as we see as the blue rim around the planet (Seager & Deming 2010).

In Figure 1.4, we can see the atmospheric annulus, in blue, when the planet transits in front of its star. So, obtaining the stellar spectrum during the planet's transit and comparing it when it is not transiting the star allows us to measure if there is any increment in the depth of the absorption lines during the in-transit-spectra, which will suggest chemical species (atoms and molecules) in the planet's atmosphere are responsible for that additional absorption lines. The difference between in-transit and out-of-transit defines the transmission spectrum,

$$\frac{F_{in} - F_{out}}{F_{out}} = \frac{F_{in}}{F_{out}} - 1 \tag{1.2}$$

Here F_{in} and F_{out} represent the in-transit stellar spectrum flux and out-of-transit stellar spectrum flux, respectively.

The idea of finding any chemical composition in the planet's atmosphere using photometric methods was first attempted by Schneider (1994). The author investigates the possibility of finding oxygen (o) absorption lines in the optical spectrum of a star when an orbiting planet partially occults it. Rauer et al. (2000) searched for chemical signatures in an exoplanet exosphere orbiting 51 Peg, the first exoplanet detected orbiting a main sequence star; however, they did not find a clear detection of absorption lines during the transit. Seager & Sasselov (2000) developed theoretical models for HD 209458b, a gas giant extrasolar planet orbiting a Sun-like star, for which the transmission spectra were estimated. They find strong absorption signatures of Na I and K I and strong signatures of He I 2 $^3S - 2\ ^3P$ triplet line at 1083.0 nm. In addition, from the transmission spectra observations, it was possible to constrain the cloud depth and the column density, temperature, and pressure of the planet's upper atmosphere. Brown (2001) investigated and described a model spectrum for planets such as HD 209458b and similar to it, he

suggested the spectra of transiting extrasolar giant planets (EGPs) can be used to infer many atmospheric properties such as cloud heights, heavy elements abundances, temperature (and temperature stratification) and wind velocities. Brown (2001) also suggest that to achieve such atmospheric properties, it is required to have high-resolution spectrographs with observations of signal-to-noise ratio (S/N) of 10^3 and a resolving power $R = \lambda/\delta\lambda$ ranging from 10^3 to 10^6 to resolve these properties.

Charbonneau et al. (2002) detected absorption lines in an exoplanetary atmosphere for the first time. They found Na I absorption lines in the HD 209458b's atmosphere using the *Space Telescope Imaging Spectrograph (STIS)* installed on the *Hubble Space Telescope (HST)*. On the other hand, Redfield et al. (2008) reported the first ground-based detection of Na I absorption lines in the transmission spectrum of HD 189733b. That detection was made using the High-Resolution Spectrograph (HRS) on the *Hobby-Eberly Telescope (HET)*. Those findings opened a new era in exoplanets atmosphere characterization. Finally, today, astronomers often combine space and terrestrial observations to characterize and study the main phenomena affecting exoplanets' atmosphere.

1.3 Planetary evolution of exoplanets

Planetary evolution remains one of the most challenging ongoing astronomical research. From the discovery of planets around a pulsar (Wolszczan & Frail 1992) to the discovery of the first exoplanet (51 Peg b) around a main sequence star (Mayor & Queloz 1995), our knowledge about the formation of other planetary systems, especially planets formation, had only just begun.

Discoveries made by the *Kepler* space telescope, for example, show a variety

of planets and a diversity of planetary systems in the Milky Way, which allows astronomers to start to develop theories about how and where planets can form. So, looking at the extremes, astronomers find hot Jupiter and super-Earths. However, planets called "hot Neptunes" are hard to find; only a few have been found so far. Therefore, understanding the phenomena involving hot Jupiters, Super-Earths, and Hot-Neptune, which play a key role as a linker between those two extremes, can give an idea of how planetary systems form and, in fact, how planet formations work (Kennedy & Kenyon 2008)

1.3.1   Mass Loss by atmospheric escape

Atmospheric mass loss is a relevant and fundamental phenomenon that shapes exoplanets' atmospheres as well as their evolution (Kubyshkina 2024). It is well known that the atmospheric mass loss follows different mechanisms. Howe et al. (2020) consider two categories for atmospheric mass loss: thermal escape and atmospheric erosion. Thermal escape occurs when molecules escape into space due to a heated atmosphere. This phenomenon can be explained by Jeans escape, hydrodynamic escape, photoionization, or photodissociation. On the other hand, atmospheric erosion occurs due to the ablation of stellar winds and impact erosion, which occurs when large bodies collide with the atmosphere. McCann et al. (2019) modeled for close-in gaseous planets undergoing hydrodynamic atmospheric escape and suggested that stellar environments significantly shape planetary outflows. They examined several components of stellar environments and found three unique stellar wind regimens. For a weak stellar wind regime, the authors found that it cannot restrain the planetary outflow, an intermediate regime causes periodic disruption of the growing planetary outflow, and strong stellar winds cause

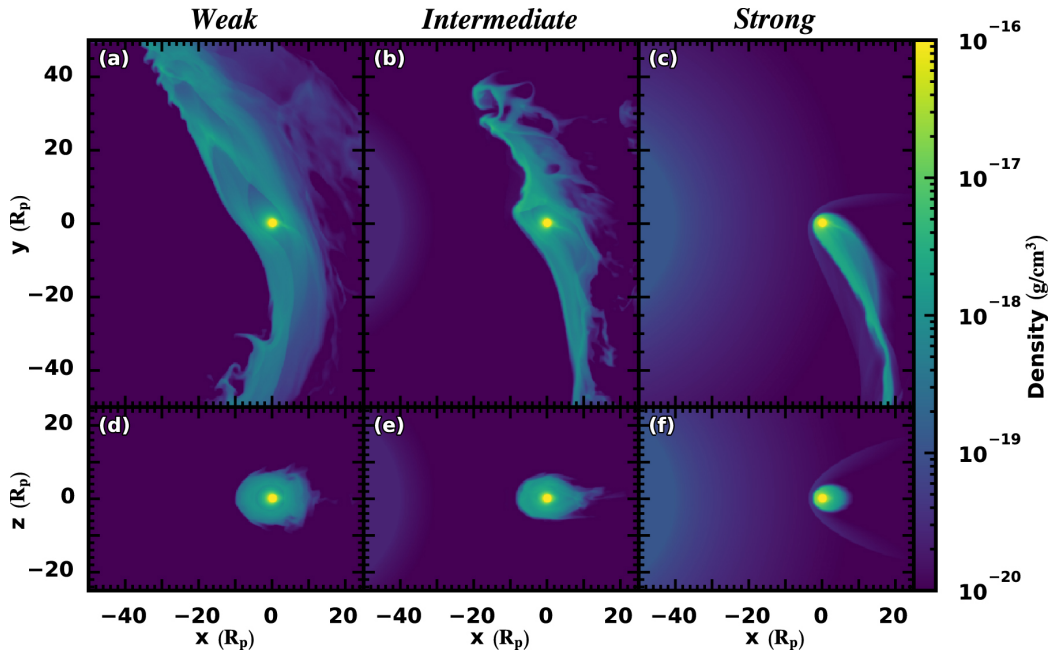planetary outflows similar to the comet tail (Figure 1.5).

Figure 1.5: The image shows hydrodynamic escaping planetary atmosphere for different wind strengths (weak, intermediate, and strong. We see how the stellar environment, due to the force of the wind, shapes the escaping planetary outflow (McCann et al. 2019)

In 2022, Koskinen et al. (2022) explored high rates of mass loss by atmospheric escape from nearby exoplanets due to the transition from stellar XUV (X-ray and ultraviolet) driven escape of the upper atmosphere to Roche lobe overflow of the middle atmosphere and also performed a detailed numerical simulation of atmospheric escape from Uranus- or Neptune-type planets orbiting near solar-type stars, to address quantitative differences between hot Jupiters and sub-Jovian planets. They found that solar-metallicity hydrogen and helium envelopes in hot Neptunes have relatively higher extended atmospheres than hot Jupiters, with a lower fraction of ionization and higher abundances of escaping molecules. Hubbard et al. (2007) observed a mass function for extrasolar giant planets (EGPs) and studied its evaporation effect for high irradiated EGPs with orbital radii <0.07

AU. They did not find a significant change in the EGPs mass, and also they did not find evidence for evaporation effects. In the same line (Murray-Clay et al. 2009) construct a model of escape that takes the form of hydrodynamic wind, finding that UV radiation, which drives winds from hot Jupiters, cannot affect the planetary mass of hot Jupiters at any evolutionary stage. Therefore, mass loss related to the atmospheric escape in hot Jupiter represents just the $\sim 1\%$ (Fortney et al. 2021) and is no longer considered a factor to drive its evolutionary track. This made astronomers start looking for smaller planets, such as Neptune-size planets.

For Neptune-type exoplanets, atmospheric escape seems to be an important factor in their evolutionary stage. However, at the current exoplanet statistics detection, astronomers have identified some of them, and studies carried out to date suggest the existence of a significant dearth of Neptune-mass planets. In 2011, Szabó & Kiss (2011) reported a lack of planets with a mass between $0.02 - 0.8$ M$_J$ and a short period ($P_{orb} < 2.5$ days). This lack of exoplanets in the period–minimum mass distribution was called the "sub−Jupiter desert." Mazeh et al. (2016) presented a larger sample to analyze short-period planets in period-mass and period-radius relationship to examine the location and shape of the desert, where they found a scarcity Neptune-size planets and called that region the "Neptunian desert". In Figure 1.6 we can see this called Neptunian desert, which is delimited by a triangular shape, where we can identify TOI-1288b a hot-Neptune type exoplanet marked in a square (Knudstrup et al. 2023).
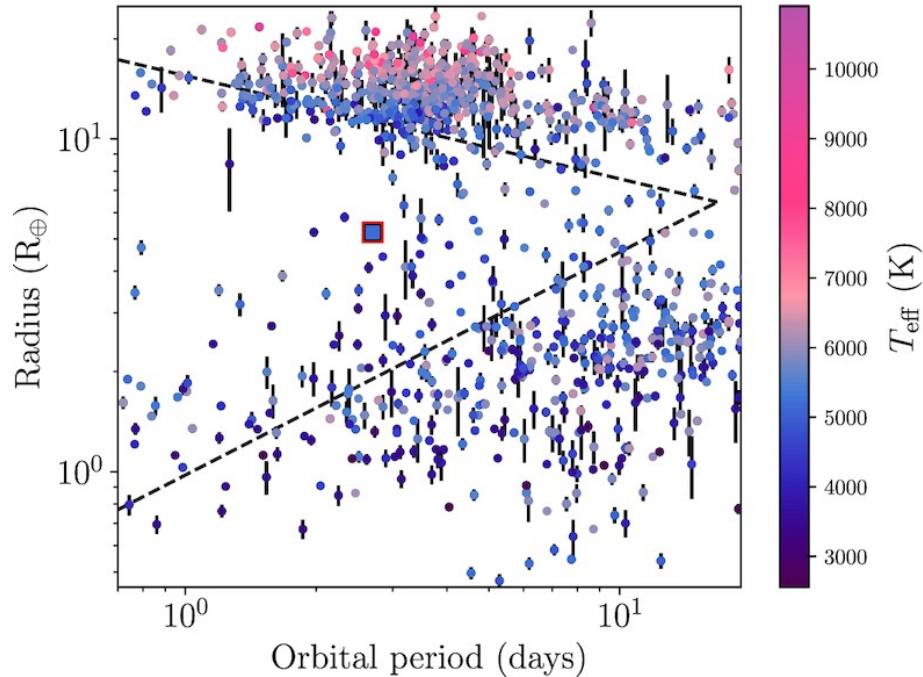
Figure 1.6: Radio vs. orbital period relationship. The "Desert of Neptune" is shown in the triangular-shaped region. As we can see, this triangular region shows a scarcity of exoplanets. TOI-1288b (super-Neptune) belongs to the Neptunian desert and is marked by a square.(Knudstrup et al. 2023)

As we see in Figure 1.6 the boundaries of the Neptunian desert are marked by large and small type exoplanets. Owen & Lai (2018) showed that this desert can be explained by photoevaporation in the atmosphere of highly irradiated sub-Neptunes, consistent with the shape of the lower boundary in the radius-period plane. Also, they showed that the upper boundary in the radius-period plane would be filled by a very short period of sub-Jovian in agreement with the observations. Szabó & Kálmán (2019) showed the boundary of the Neptunian desert depends on the fundamental stellar parameters, where photoevaporation plays a fundamental role in forming the desert. Magliano et al. (2023) presented an analysis of 250 transit-like events in the *TESS* inside of the Neptunian desert, with P $\leq$ 4 days and $3R_{\oplus} \leq R \leq 5\,R_{\oplus}$, identified 18 hot Neptune-sized candidates. From

that analysis, we noticed the Neptuanian desert cannot be explained by observational biases because planets with Neptune's radius and mass with longer periods have been observed. So, using radial velocity and transit surveys, Neptunian-sized planets with short periods should be easier to detect.

1.3.2   Hα detection in the exoplanet extended atmosphere

Detection of absorption lines in an exoplanet atmosphere allows us to characterize and better understand the planet itself. The Hα line is one of the interesting markers to characterize exoplanets' atmospheres. In 2004, Winn et al. (2004) searched for Hα in HD 209458b atmosphere using the Subaru High Dispersion Spectrograph. Despite the presence of neutral hydrogen in HD-209458b, they could not detect Hα absorption lines. In 2012, Jensen et al. (2012) made the first Hα detection in an exoplanet atmosphere using the High-Resolution Spectrograph (HRS) on the *Hobby–Eberly Telescope (HET)*. Yan & Henning (2018) reported a detection of Hα envelop in a hot giant exoplanet (KELT-9b) using CARMENES, a high-resolution spectrograph. On the other hand, Wyttenbach et al. (2020) also detected and analyzed the Hα absorption line in the upper atmosphere of KELT-9b using high-resolution transit observations with HARPS-N. They suggested hydrogen is filling the planetary Roche lobe and escaping from the planet. Bello-Arufe et al. (2023) presented the first analysis of the atmosphere of the low-density Saturn-mass exoplanet (HAT-P-67b) with CARMENES spectrograph. In addition, they explored the potential atmospheric escape of Hα and the metastable helium line.

All detections of Hα in the papers listed above were performed using the transmission spectroscopy method. So, due to the success of this technique in

detecting absorption lines, we will perform it further in Chapter 3.

1.4   TOI-1288 planetary system

As we saw in the previous sections, the Milky Way has different planetary systems. We will look at the TOI-1288 planetary system, which is formed by a late G dwarf star that hosts the planets TOI-1288b and TOI-1288c (Knudstrup et al. 2023). In this thesis, we will focus on the search for the 6562.8 Å of H-alpha (Hα) absorption line in the TOI-1288b extended atmosphere and attempt to understand way detections or nondetections of Hα.

TOI-1288 was observed by *TESS* (Sectors 15, 16, 17, 18, and 24);(Jenkins et al. 2016). In 2021, TOI-1288 was listed in the TESS Objects of Interest (TOI) Catalog because its light curve showed a drop of $\sim 0.25\%$, every 2.7 days (Guerrero et al. 2021). Later, using *TESS* photometry and ground-based telescopes Knudstrup et al. (2023) reported and confirmed the planetary system TOI-1288.

Table 1.1 shows the stellar parameters of TOI-1288. Knudstrup et al. (2023) measured those parameters from spectral analyses and stellar modeling. They performed high-resolution reconnaissance spectroscopy using the FIber-fed Echelle Spectrograph (FIES) and used the High Accuracy Radial Velocity Planet Searcher-North (HARPS-N) to derive stellar properties with the software SME (Spectroscopy Made Easy) and the spectral energy distribution (SED). They also modeled the star using the BAyesian STellar Algorithm (BASTA).

Knudstrup et al. (2023) found the planetary parameters of TOI-1288b as is listed in Table 1.2. So, to measure TOI-1288b properties, the authors applied the Markov Chain Monte Carlo (MCMC) code. From the results, it was found that the planet is a hot super-Neptune with a period of ~ 2.7 days around its host

Parameter	Value
Distance (pc)	114.7 ± 0.7
Stellar Radius ($R_\odot$)	$1.010^{+0.015}_{-0.014}$
Stellar Mass ($M_\odot$)	$0.65^{+0.14}_{-0.13}$
Effective temperature, T_{eff} (K)	$5225^{+0.23}_{-0.27}$
Age (Gyr)	$12.1^{+1.4}_{-3.1}$
Spectral type	G
V magnitude	10.44 ± 0.04
Surface gravity (log g)	4.24 ± 0.09
Iron abundance ($[F_e/H]$)	0.07 ± 0.09

Table 1.1: Stellar parameters of TOI-1288 from Knudstrup et al. (2023)

star. Therefore, due to its properties, TOI-1288 b falls into the Neptunian desert. As we mentioned in Section 1.3.1, planets localized in the Neptunian desert are the link between small and large mass exoplanets, and they are also excellent candidates to study their evaporating atmospheres. Therefore, searching for a Hα in TOI-1288 b will provide us an insight into its planetary evolution (see Chapter 3).

Parameter	Value
Period (days)	$2.699835^{+0.000004}_{-0.000003}$
Planet Radius ($R_\oplus$)	5.24 ± 0.09
Planet Mass ($M_\oplus$)	42 ± 3
Equilibrium temperature (K)	1266 ± 27
Planet density (g cm^{-3})	1.3 ± 0.5
Inclination (degrees)	$88.3^{+1.7}_{-0.07}$
Transit duration (hours)	$2.37^{+0.05}_{-0.03}$

Table 1.2: Planetary Parameters of TOI-1288b from (Knudstrup et al. 2023)

Chapter 2

Observing TOI 1288

Our main objective is to search for Hα signatures in the extended atmosphere of TOI 1288b by comparing the in-transit and out-of-transit spectra of TOI-1288. In-transit spectra are obtained when the hot super-Neptune passes between the observer and the star. All other spectra are considered out-of-transit. Comparing the spectra will allow us to search for a decrease in the 6562.8 Å Hα absorption line. Suggesting the presence of an escaping atmosphere in TOI 1288b.

We use data from the High Accuracy Radial Velocity Planet Searcher for the Northern Hemisphere (HARPS-N), a ground-based spectrograph attached to Telescopio Nazionale Galileo (TNG) in the Canary Islands, Spain.

In this chapter, we describe the observations and make an initial examination of the data to identify the Hα absorption lines, the signal-to-noise ratio, and the determination of the in and out-of-transit exposures.

2.1 HARPS-N

HARPS-N is a visible-light spectrograph installed at the Italian Telescopio Nazionale Galileo, a 3.58-meter telescope located at the Roque de los Muchachos Observatory on the island of La Palma, Canary Islands, Spain.

The HARPS-N design is based on its predecessor working at ESO's 3.6m telescope at La Silla Observatory in Chile. The spectrograph was designed to allow

measurement under 1 m s^{-1}, which will enable the characterization of rocky, Earth-like planets (Cosentino et al. 2012). The instrument covers the wavelength range from 3800 to 6900 Angstrom with a resolving power of $R \simeq 115000$ (Nardetto et al. 2023). We can calculate the wavelength resolution at the 6562.8 Å line using the formula given in Chromey (2016),

$$R = \frac{\lambda}{\Delta\lambda} \tag{2.1}$$

where λ is the wavelength of observation and $\Delta\lambda$ is the wavelength bin size. Then, from Equation 2.1 we calculate $\Delta\lambda \approx 0.05$ Å, which means that the HARPS-N can spatially resolve a Hα line of width 0.05 Å.

The spectrograph is a fiber-fed, cross-dispersed echelle. Two fibers, an object and a reference fiber of 1 arcsec aperture, pick up the light at the Nasmyth B focus of the telescope and feed the spectrograph either with calibration or stellar light. The fiber entrance is reimaged by the spectrograph optics onto 4k×4k CCD, where echelle spectra of 69 orders are formed for each fiber. The fiber diameter gives the resolution of the spectrograph, and for that resolution, each spectral element is sampled by 3.3 CCD pixels (Cosentino et al. 2012).

Figure 2.1 shows a HARPS-N schematic view, where the spectrograph is located on the ground floor of the telescope, operating in a vacuum environment.
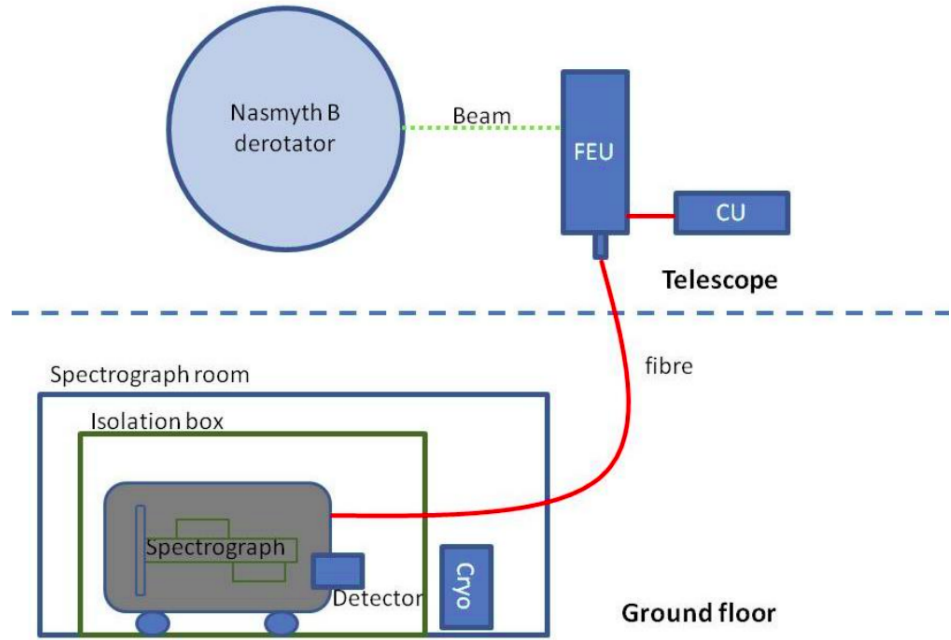
Figure 2.1: HARPS-N general schematic view (Cosentino et al. 2012)

2.2   Data collection

Observations of TOI-1288 were taken from July 21 to 22, 2020 UT, covering the entire planet transit of 2.37 hours with eight 30-minute exposures and one 24-minute exposure, totaling 9 exposures. These observations were taken to observe a Rossiter-McLaughlin (RM) effect occurs during the planet's transit. The RM provides the main means of measuring the sky-projected spin-orbit angle between a planet's orbital plane and its host star's equatorial plane (Triaud 2018).

We use the `batman` package from Kreidberg (2015) to plot a model of TOI-1288b's light curve during a transit, obtaining the light curve phase of the transit. To get Figure 2.2 requires parameters such as the planet's radius, its orbital period, and the limb darkening coefficients. Depending on the given limb darkening coefficients, the bottom transit curve changes, ranging from a square to an oval

Date (UT)	Time (UT)	In vs. Out Transit	Average SNR
2020-07-21	22:27:09	Out	69.5
2020-07-21	22:57:35	Out	68.6
2020-07-21	23:28:01	In	64.7
2020-07-21	23:58:27	In	64.2
2020-07-22	0:28:53	In	61.6
2020-07-22	0:59:19	In	60.8
2020-07-22	1:29:44	In	60.4
2020-07-22	2:00:09	In	55.9
2020-07-22	2:30:35	Out	46.6

Table 2.1: TOI-1288 observations

shape. Stellar limb darkening is a wavelength-dependent dimming of the surface brightness from the center of the stellar disk to the limb. Using equations from Kipping (2013) and variants from Knudstrup et al. (2023), we determined the limb-darkening coefficients. In addition, using `Tapir` from Jensen (2013) we reaffirmed which exposures are taken in-vs-out of transit (See Section 2.4 for more detail).

TOI-1288 observations were taken from July 21 to 22, 2020 UT. Table 2.1 details the individual exposures taken for it. The table columns show the date and time of the observation, as well as which observations are in-transit or out-of-transit. For more details on the signal-to-noise ratio column, see Section 2.3.
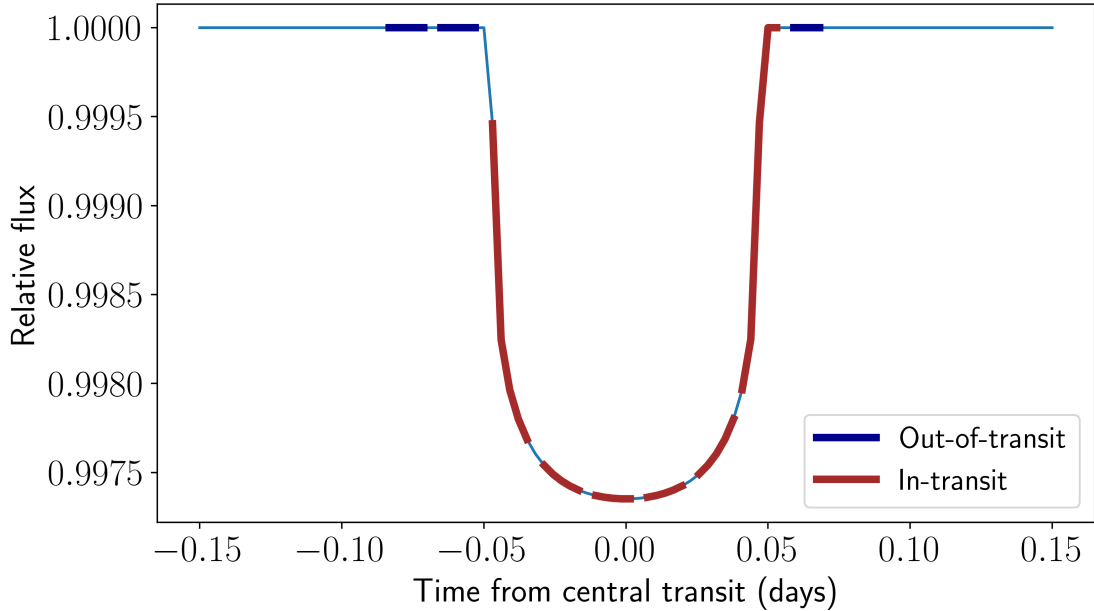
Figure 2.2: Phase light curve plot of TOI-1288b transit. Transit model made using the `batman` package from Kreidberg (2015). The blue lines and red lines represent the out-of-transit and in-transit, respectively.

2.3   Analyzing the SNR

All astronomical signals involve some associated noise or error. This noise could be any surrounding source close to the target or be a systematic noise due to an increment in the instrument temperature. So, we can define the signal-to-noise ratio (SNR) as the comparison of the number of photons detected from a source (Signal) with the total random contribution from counting statistics (Noise). Here, we analyze the SNR for each observation using the following equation.

$$\text{SNR} = \frac{\text{Signal}}{\text{Noise}} = \frac{\text{Flux}}{\sqrt{\text{Flux}}} \tag{2.2}$$

Figure 2.3 displays the signal-to-noise for each exposure in our data, where the red spectra correspond to the in-transit while the blue ones correspond to the out-

of-transit exposures. We performed it using Equation 2.2. As we see, the shape of the SNR correlates with the shape of the science spectrum. We calculated the average of the signal-to-noise ratio (see Table 2.1). Therefore, we identified the low and high SNR exposures from the inspection of the figure and table. Here, 46.6 is the low SNR exposure, which corresponds to out-of-transit exposure, and 69.5 is the high SNR, which also corresponds to out-of-transit. The in-transit exposures almost have a similar SNR, except for one of them (SNR = 55.9). This exposure corresponds to the last of in-transit exposure, going from the top to the bottom in the figure, which also has a small part of it out-of-transit. (see Figure 2.2).
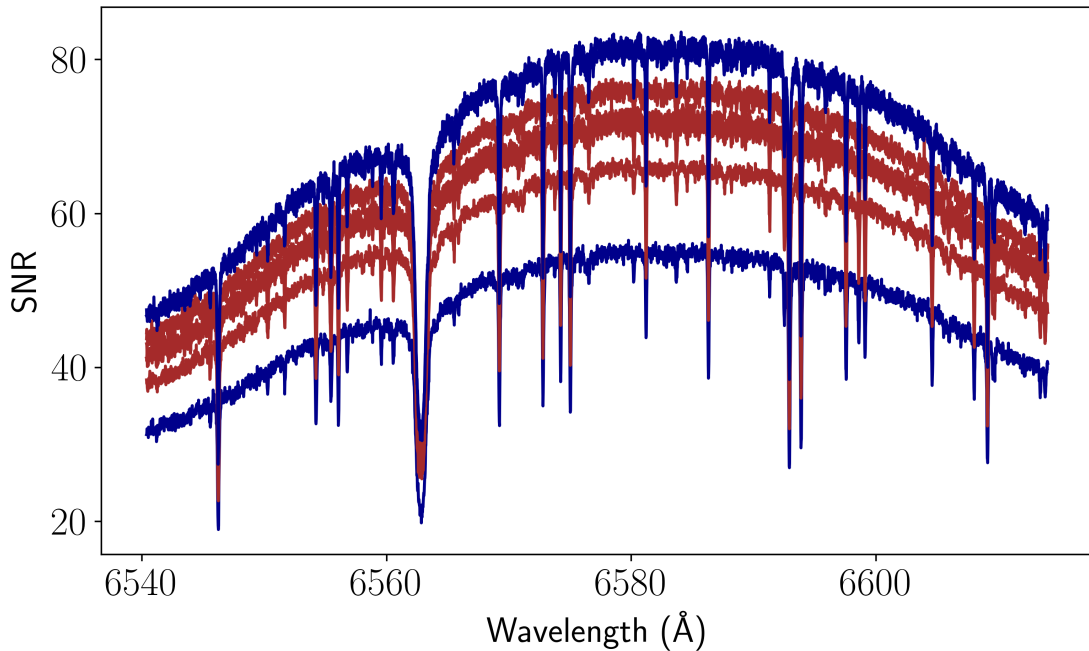

Figure 2.3: SNR of each exposure spectrum of TOI-1288. The SNR extremes are in blue and correspond to out-of-transit exposures, while in-transit exposures are in red.

2.4 Determining in-transit and out-of-transit observations

Determining which of the exposures happened when TOI-1288b was passing in front of its star and which of them were when the planet was not is one of the important steps before beginning with the data analysis. In section 2.2, we determined the light curve phase of the TOI-1288b, and to corroborate it, we used a web interface, `Tapir`. This is used for planning follow-up visible observations from given locations on given days of periodic targets such as eclipsing binaries and transiting planets. It uses orbital and planetary parameters from the NASA Exoplanet Archive database (Jensen 2013)

From the transit duration and the given time for each exposure, we determine the corresponding in-transit and out-of-transit, which agrees with the `Tapir` database results. Table 2.1 shows in detail the day, time, SNR, and In and out transit of each observed exposure.

Finally, after determining the in-transit and out-of-transit exposures, we are ready to dive into the data analysis to determine if there is a planetary Hα signature in TOI-1288b extended atmosphere at 6562.8 Å.

Chapter 3

The Transmission Spectrum

In Chapter 2, we determined the exposures corresponding to the in-transit and out-of-transit. By comparing them, we will be able to obtain the transmission spectrum of the Hα absorption line. This analysis will indicate the presence or absence of Hα in the extended atmosphere of TOI-1288b. We will perform the barycentric correction to ensure we are looking at the Hα line and compare the in-transit and out-of-transit to arrive at the transmission spectrum. In addition, we will propagate the error in our measurements. Therefore, this chapter will describe the steps to obtain the transmission spectrum, which will be further analyzed in the following chapter.

3.1 Barycentric correction

To determine the location of the Hα line in our spectrum, it is necessary to consider the motion of the Earth and the motion of the star. This means subtracting the velocity of the telescope (due to the orbital and rotational motion of Earth) in the direction of the star from the measured velocity to get the star's velocity with respect to the solar system (Wright & Kanodia 2020). To start with our barycentric correction, we use the pyastronomy library `Helcorr`; this function is imported from the `REDUCE IDL` package developed by Piskunov & Valenti (2002). This function calculates the motion of an observer in the direction

of a star, which considers Earth's motion, including its rotation relative to the solar system.

The required parameters to get the correction are the observation location on the Earth, star coordinates, and the Julian date for the middle of the exposure. Figure 3.1 shows the barycentric correction in a radial velocity domain.
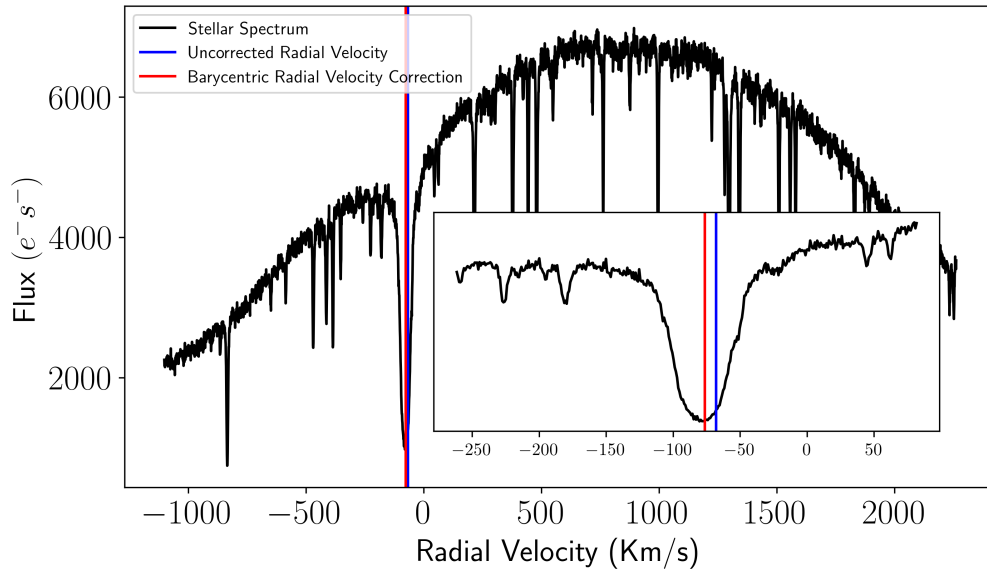

Figure 3.1: TOI-1288 barycentric radial velocity correction for line Hα. The red and blue lines correspond to the star's corrected and uncorrected radial velocity, respectively.

However, to get the barycentric correction in the wavelength domain, we need to use the Doppler formula,

$$\frac{\triangle\lambda}{\lambda} = \frac{v}{c} \tag{3.1}$$

where v is the radial velocity and c is the speed of light. We look at TOI-1288 radial velocity is $v = -68.1$ km s^{-1} (Knudstrup et al. 2023) and we got its radial velocity correction in the rest frame at $v \approx -76.32$ km s^{-1}. Therefore, using the Equation 3.1, we obtained $\triangle\lambda$ at wavelength rest frame as shown in Figure 3.2, which shows the correction for Hα. Furthermore, this correction also works for

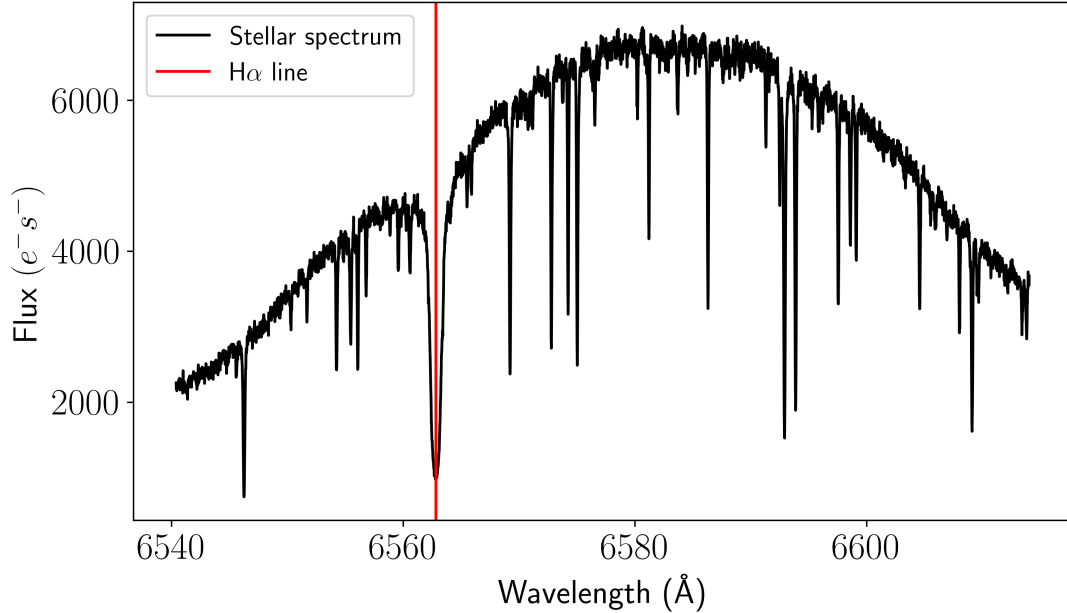all other lines in the 3800 to 6900 Å of the HARPS-N spectrum.

Figure 3.2: Stellar spectrum at the rest frame. Here, the x-axis has been converted to the wavelength domain at its shows, where the red line matches the Hα absorption line

3.2   Normalization around Hα line

The first step in obtaining the transmission spectrum from our data is the spectrum's normalization. This normalization is because we are working at differential measurements in wavelength. Here, we focus especially on normalizing our spectrum around the Hα absorption line. We used the least squares polynomial fit (`polyfit`) in a one-dimensional polynomial (`Poly1d`) class. Because Hα is a strong absorption line in the spectrum, we had to use a `sigma_clip` to get a better fit and normalization around the Hα line.

`sigma_clip` is an `Astropy` package that works in a distribution of points, calculating the center and its standard deviation. Therefore, at each interaction

of this function, react values that are less or more than a specific number. We performed this function three times in order to get rid of all the absorption lines. We clipped almost 85% of the absorption lines the first time and the last two around 10% and 5%.

Figure 3.3 follows the steps to normalize the spectrum; as we can see in each interaction, we improve the normalization of the spectrum (red line). Additionally, we used different polynomial degrees in each clipping to achieve a better normalization every time. Therefore, the combined method of clipping and polynomial fitting curve gives a decent spectrum normalization around the Hα absorption line.
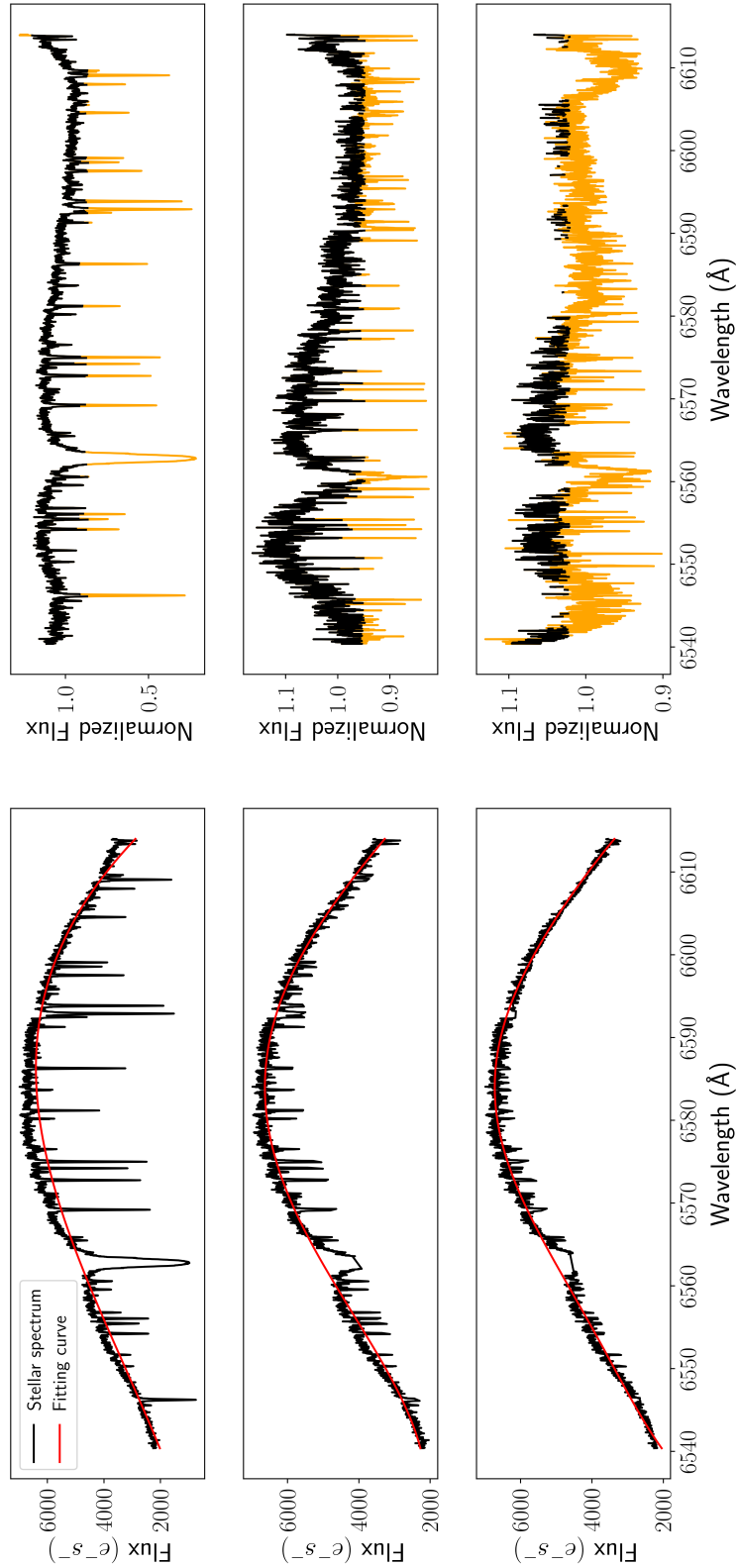
Figure 3.3: Stellar spectrum fitting and clipping around Hα line. *leaft*: Unormalized spectrum and the polynomial normalization fit in red. *Right*: Normalized spectrum, where the clipped points are in orange.

Figure 3.4 shows the last polynomial fitting model around the line Hα. As we can notice, the top graph shows the fit on the spectrum, and the middle graph is a close-up of the top graph around Hα, where the fit looks quite good. So, after ensuring our fit works and as a final step, we perform normalization of the spectrum around the Hα line as shown in the bottom graph.
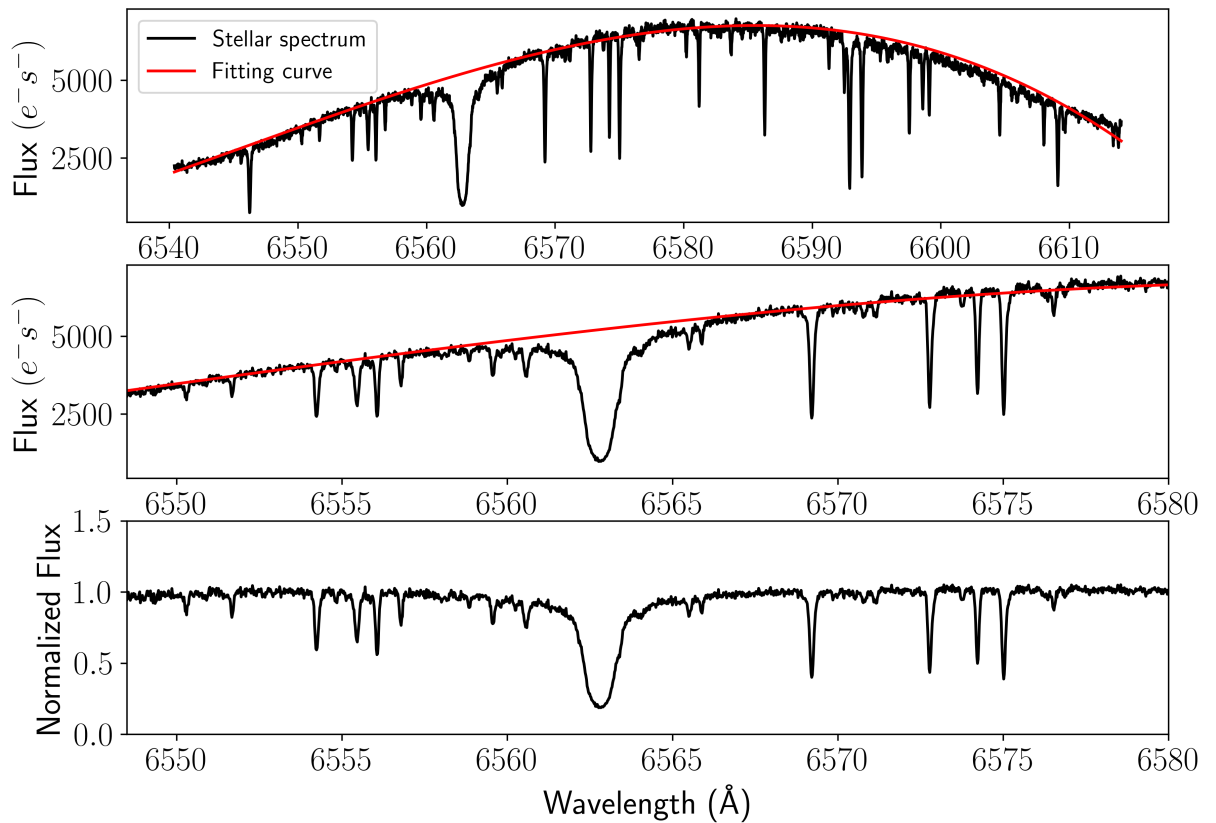

Figure 3.4: Last fitting and final normalization of stellar spectrum around Hα line. *Top*: Fitting model on the stellar spectrum. *Middle*: Zoom in on the fitting around the Hα line. *Bottom*: Hα normalization.

3.3   In-transit and out-of-transit

We determined the in-transit and out-of-transit exposures from our date in Chapter 2. In the previous section (Section3.2), we obtained the normalization steps around the Hα line in the spectrum. Then, applying the normalization method developed in our observation for each exposure, we can compare all of the in-transit and out-of-transit exposures. Figure 3.5 shows the in-transit and out-of-transit around Hα absorption line, where Hα is marked by the blue dashed line. At first look, we can say that the red and black lines, the in-transit and out-of-transit, respectively, almost match perfectly. Therefore, this first result suggests that there is no Hα absorption caused by the atmosphere of TOI-1288b. However, we will be able to confirm this result when we obtain the transmission spectrum for TOI-1288b in Section 3.5.
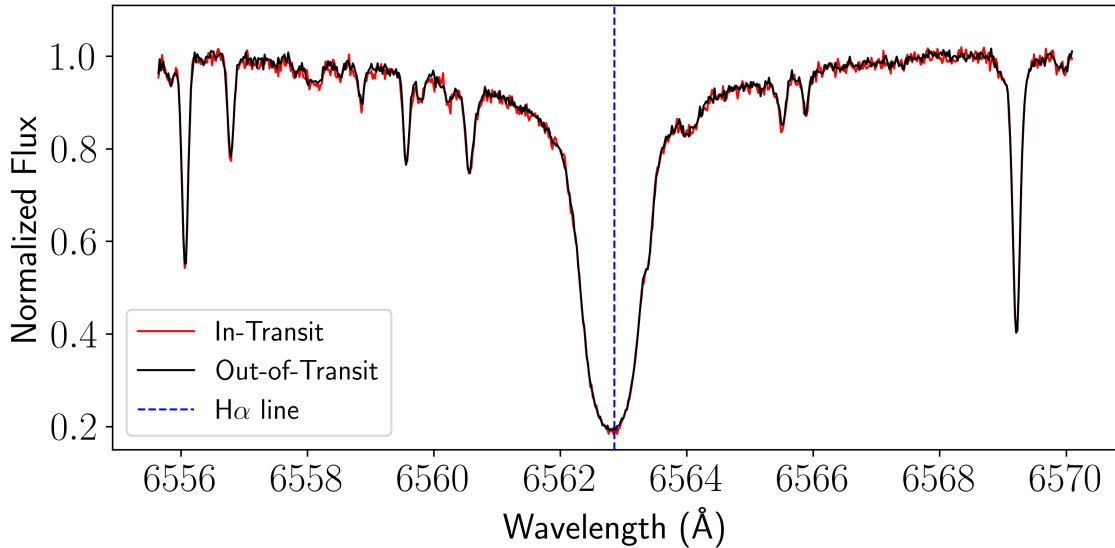

Figure 3.5: Stellar in-versus-out transit spectrum. The sum of the exposures of in-transit and out-of-transit, respectively, seems to match. No planetary Hα, absorption line signal, is visible.

3.4   Error propagation

We performed an error propagation analysis of our data. We started calcu-
lating the error for each of our exposures and calculated the error propagation
following Bevington & Robinson (2003), where the propagated error, σ_{total}. Then,
uncertainty due to the error propagation is defined by,

$$\sigma_{total}^2 = \sum_i \sigma_i^2 \left(\frac{\partial f}{\partial x_i} \right)^2 \tag{3.2}$$

where f is a function, x_i is the variables contained within that function and σ_i^2
is the variance associated with each x_i. We performed the propagation error for
the Transmission Spectrum to obtain the uncertainties related to our calculation.
Therefore, the next section will show the transmission spectrum for Hα and its
uncertainties.

3.5   Transmission spectrum

Developing the transmission spectrum is the final step in determining any Hα
signature in TOI-1288b's extended atmosphere. We will determine the transmis-
sion spectrum using the in-transit and out-of-transit relationship in the following
way,

$$\frac{F_{in} - F_{out}}{F_{out}} = \frac{F_{in}}{F_{out}} - 1 \tag{3.3}$$

where F_{in} and F_{out} are the in-transit flux and out-of-transit flux, respectively.
Figure 3.6 shows the transmission spectrum for TOI-1288b; as we see, the y-axis
is defined by Equation 1.4 while we keep the wavelength for the x-axis. Here, we
observe some emission points in the spectrum, corresponding to two out-of-transit

exposures. Therefore, to understand those points, we analyzed the transmission spectrum.
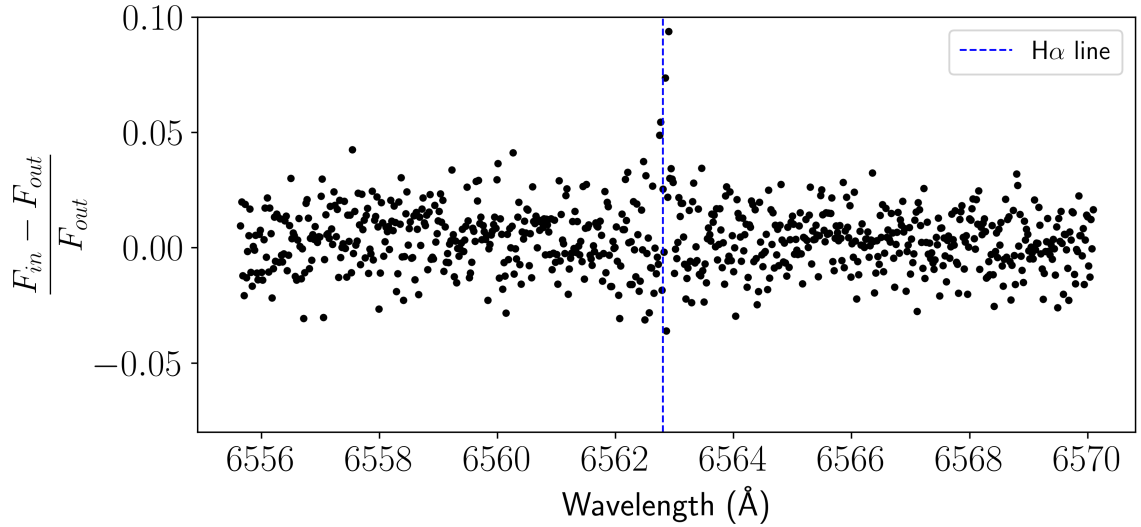

Figure 3.6: Transmission Spectrum in the planetary frame, zoomed in on the Hα wavelength region. The spectrum is flat, suggesting there is no planetaryHα in the extended atmosphere of TOI-1288b.

We applied the propagation error described in Section 3.4 to our transmission spectrum, where the propagated error value equals 0.0195. Figure 3.7 displays this error propagation for some points to visualize error bars clearly. On the other hand, we also performed a histogram analysis (See Figure 3.8) of the transmission spectrum in order to visualize the data distribution around Hα. We measured its mean ($\bar{m}$) and its standard deviation (σ) being these values: $\bar{m} = 0.00381$ and $\sigma = 0.0138$. Therefore, comparing the propagation error and the standard deviation, we see that those numbers are quite similar.
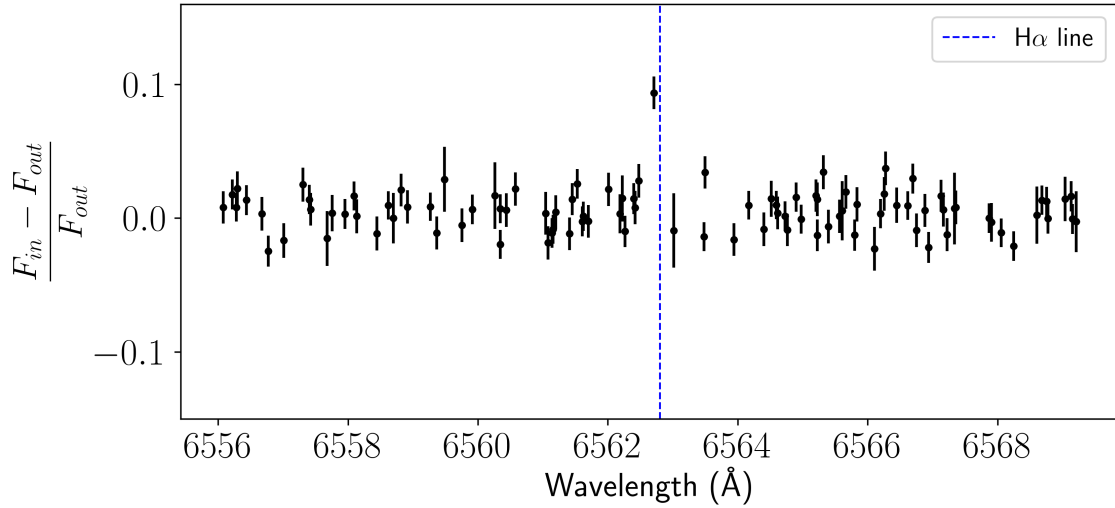
Figure 3.7: Transmission spectrum in the planetary rest frame depicting propagated error. We plot some points to improve the region's error visualization. The spectrum is flat, suggesting there is no planetary Hα in the extended atmosphere of TOI-1288b.

So, as we see in Figure 3.8, the solid black line is the mean of the transmission spectrum, and the dashed lines correspond to its standard deviation. The data limits for Figure 3.8 around Hα range from 6555 to 6570 Å (See Figure 3.6), where the data shows a smooth Gaussian histogram shape, indicating that we did a suitable normalization.

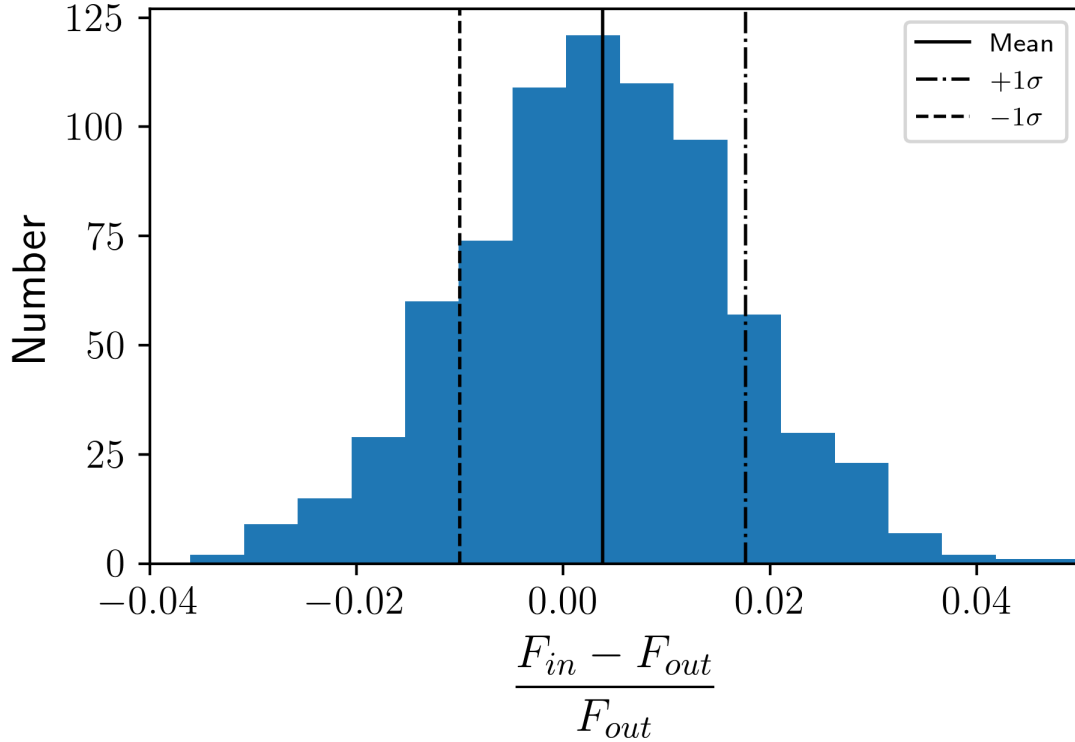**Figure 3.8:** Histogram distribution of the transmission spectrum. The solid line is the Mean of the distribution, and the dashed lines are the standard deviation of it.

Finally, from Figure 3.6 and the analyses in this section, it is apparent that there is no obvious planetary Hα absorption. We see a flat spectrum, which suggests that there is no Hα absorption signature in the extended atmosphere of TOI-1288b.

3.6   Telluric correction

As a following step, we need to check for the Earth's atmospheric absorption because we are using a ground-based telescope. Earth's atmosphere contains 78% nitrogen, 21% oxygen, and 1% other gases. Therefore, our spectra contain and can be contaminated for those lines.

Figure 3.9 shows an Earth's atmospheric lines around 6562.8 Å and TOI-1288

stellar spectra, where we used SKYCALC (Sky Model Calculator) to obtain the Earth's telluric lines. Comparing both spectrums, we see two telluric lines matching in the stellar spectrum. We searched for those absorption telluric lines in all our exposures and found them in all of them. An interesting feature we detected is that telluric lines do not change for all our exposures, which means those do not change during the whole observation time. Therefore, we can remove those telluric lines in the in-transit and out-of-transit derivation.
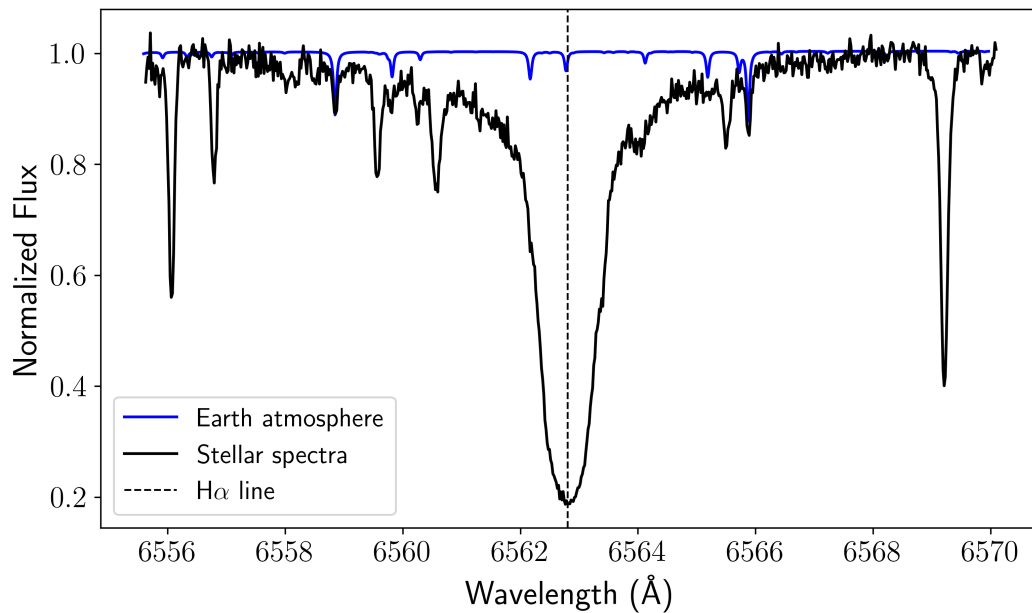
Figure 3.9: TOI-1288 stellar and Earth's atmospheric spectra around Hα absorption line.

In Figure 3.10, we overploted the telluric lines and the transmission spectrum. Looking at the figure, we do not see any telluric pattern in the transmission spectrum. Therefore, those were removed successfully in the in-transit and out-of-transit derivation.
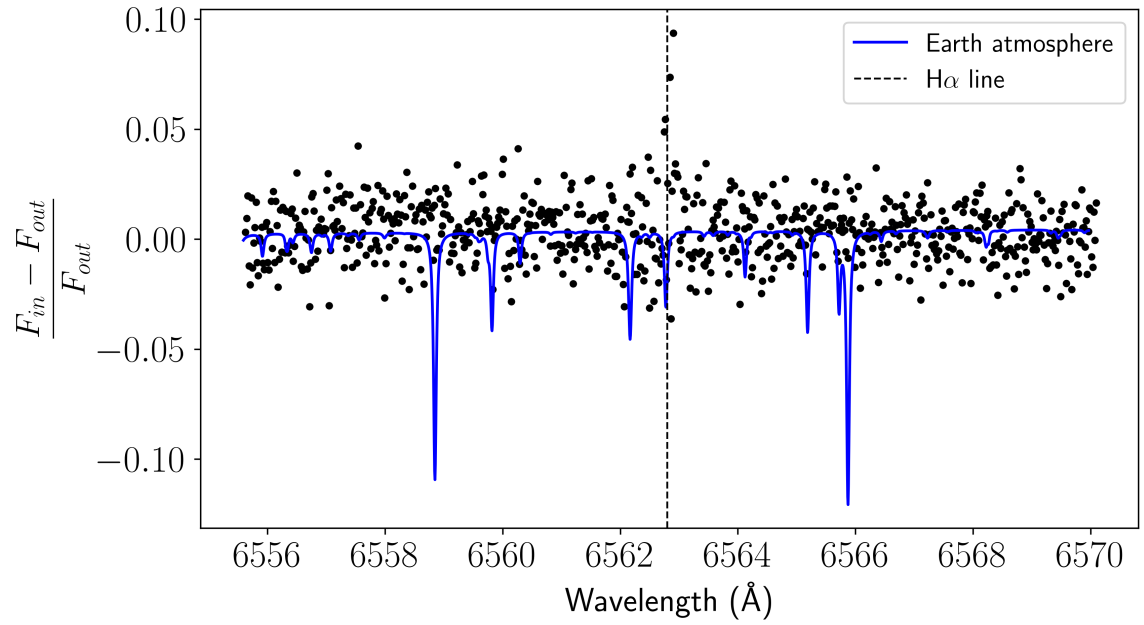
Figure 3.10: Transmision spectrum and telluric lines. There are no telluric lines in the TOI-1288b transmission spectrum.

Chapter 4

Calculating And Analyzing Our Results

In this chapter, we will develop an analysis of the TOI-1288b transmission spectrum to explain the results in Chapter 3. We will try to give a reasonable explanation for the flat transmission spectrum seen in Figure 3.6. This analysis will help us to understand the implication of detection and non-detection of Hα absorption line in the hot super-Neptune extended atmosphere. Therefore, we will calculate its absorption value.

4.1   Upper limit on Hα absorption

Although we did not observe an Hα absorption signature in the flat transmission spectrum, we need to calculate an absorption value and determine its statistical significance.

We follow the error propagation theory described in Section 3.4 to calculate the average of Hα absorption and its associated error. We decided to follow this analysis because we do not see any visible signature of Hα.

We chose 6Å and 16Å bandpasses to determine the Hα upper limit in our transmission spectrum to compare these values with the results found by Jensen et al. (2012). Table 4.1 shows the Hα absorption results of TIO-1288b equal to (4.4

Planet	16 Å Band	6 Å Band	Detection
HD 147506b	$(-4.90 \pm 1.75) \times 10^{-4}$	$(-2.87 \pm 4.97) \times 10^{-4}$	No
HD 149026b	$(3.07 \pm 1.53) \times 10^{-4}$	$(7.76 \pm 4.20) \times 10^{-4}$	No
HD 189733b	$(-10.6 \pm 2.43) \times 10^{-4}$	$(-30.2 \pm 6.33) \times 10^{-4}$	Yes
HD 209458b	$(0.503 \pm 0.802) \times 10^{-4}$	$(6.91 \pm 2.01) \times 10^{-4}$	No
TOI-1288b	$(3.45 \pm 0.14) \times 10^{-4}$	$(4.4 \pm 0.38) \times 10^{-4}$	No

Table 4.1: Comapartive table of Hα absorption results of TIO-1288b at 16Å and 6Å bands with Hα absorption results from Jensen et al. (2012)

$\pm$ 0.38) $\times$ 10^{-4} and $(3.45 \pm 0.14) \times 10^{-4}$ at 6Å and 16Å bandpass respectively. Then, by comparing those absorption limits of Hα, we can suggest that the found values are close to the values determined by Jensen et al. (2012). And therefore, we can determine the Hα upper limit (3σ), which is equal 1.14×10^{-4} and 0.42×10^{-4} at 6Å and 16Å respectively. In addition, we tested our analysis for different bandpasses by slightly increasing or decreasing the wavelength ranges, which did not meaningfully impact our final absorption value and error. Therefore, we can say that our analysis determining the absorption of Hα is within acceptable limits.

4.2 Hα absorption model on TOI-1288b extended atmosphere

Jensen et al. (2012) made an observational detection of Hα signature in HD-189733b exoplanetary atmosphere. This observational detection requires high-resolution spectrographs and telescope time to observe an exoplanet depth transit. Therefore, by developing models of the exoplanet's atmosphere, we can have a sign and model a line profile for any element that could be present in the exoplanet atmosphere. Christie et al. (2014) developed a model for the Hα extended

atmosphere of HD-189733b to compare their model with the observational profiles shown in Jensen et al. (2012). Figure 4.1 shows the models developed by Christie et al. (2014) for HD-189733b. This image shows two models where the dashed line has a low ionized profile while the continuum line has a higher ionized profile, which shows the Hα profile as it is shown for the observational profile. So, modeling line profiles in exoplanets' atmosphere provides important constraints for detecting or not detecting atmospheric signatures.
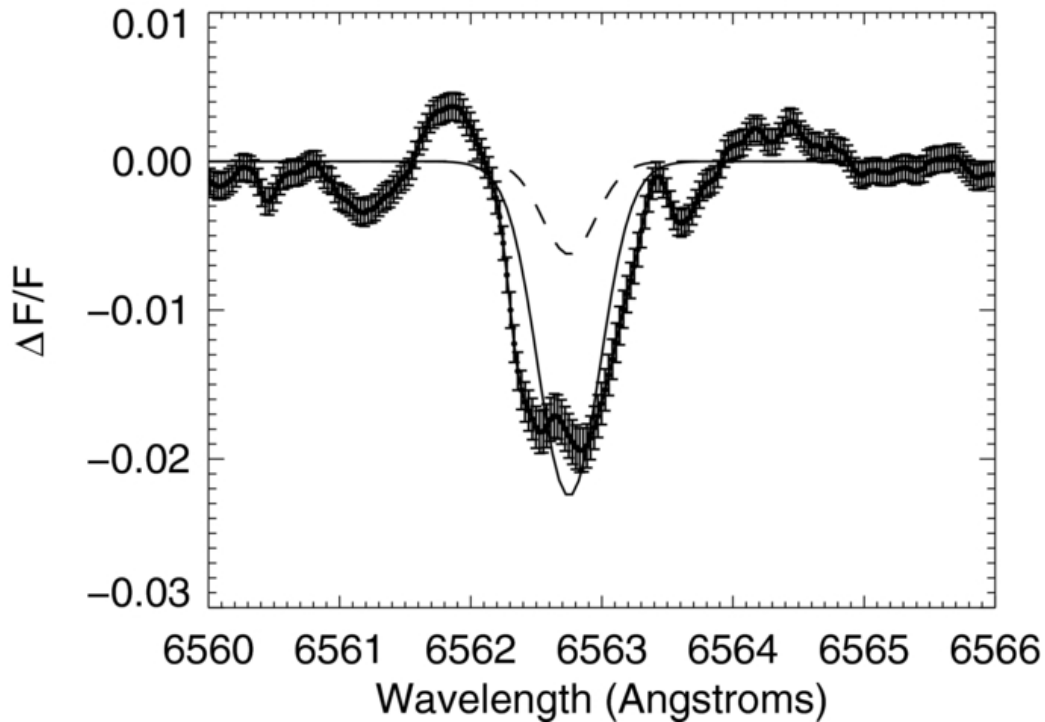
Figure 4.1: Model and observational profile of Hα absorption line of HD-189733b (Christie et al. 2014)

Modeling a line profile in the exoplanet atmosphere requires fundamental parameters related to the star-planet system. The planet's mass, radius, and impact parameter are the planet's parameters. A star's parameters are also required: mass, radius, and XUV flux. In addition, it is also essential to consider the distance between the star and its planet.

Vidotto & Cleary (2020) simulated models for close-in giant planets and investigated conditions for atmospheric escape. Vidotto simulated two models for this research, as shown in Figure 4.2. The parameters for TOI-1288 and its planet were taken from Knudstrup et al. (2023). The XUV (X-rays and extreme ultraviolet, EUV) flux reaching the planet was estimated from Rao et al. (2021). The XUV flux for each of the models are $\sim 1.3 \times 10^{-6}$ L$\odot$ (model 1) and $\sim 5.9 \times^{-5}$ L$\odot$ (model 2). Where the estimated hydrodynamic escape for each of the models is 1.8×10^{10} g s^{-1} and 3.9×10^{11} g s^{-1} respectively. Due to planets being immersed in the magnetized wind of their host stars, this interaction increases planet temperature, especially gas giant planets that orbit very close to their hosts. Vidotto adopted a temperature for both models equal to T $= 8000$K, which follows the criteria from Huang et al. (2017) and Villarreal D'Angelo et al. (2021).

We also applied the error propagation related to Vidotto's models, corresponding to 1.8Å bandpass in our data. Finding the Hα absorption value equals $(48.5 \pm 1.31) \times 10^{-4}$. Finally, from our analysis in this Section and Section 4.1, we are ready to discuss in Chapter 5 the implications of the non-detection of the Hα absorption line in the extended atmosphere of TOI-1288b.
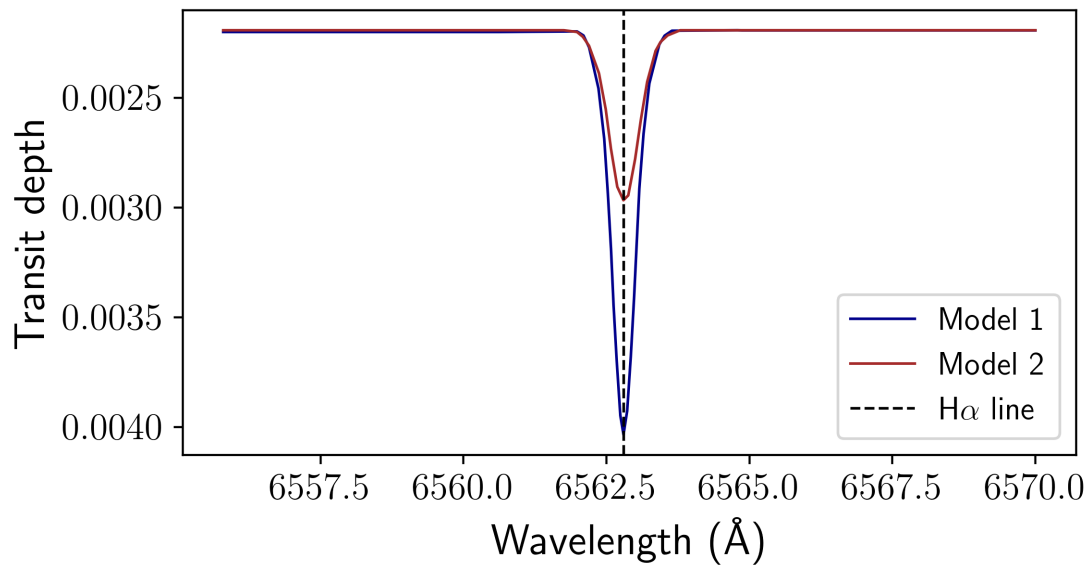
Figure 4.2: Models of Hα profiles for TOI-1288b extended atmosphere. The two curves in red and blue show the Hα absorption line estimation for the planet.

Chapter 5

Atmospheric Hα Detection and No-detection

In this chapter, our main focus is to discuss the implications of our results and analysis in Chapters 3 and 4. We start this Chapter by concluding that there is no Hα detection in the transit observation of TOI-1288b extended atmosphere. Therefore, now we will try to understand the non-detection of the Hα absorption line, considering all Hα detection and non-detection at the current time.

5.1   Stellar activity and planetary atmosphere

In Section 1.3.1, we refer to that planets lose mass due to different radiation mechanisms. Stellar magnetic activity is significantly important during the formation and evolution of planetary atmospheres and their surface conditions because the magnetic fields cause the outer atmosphere of stars to be heated to million-degree temperatures, leading to the emission of X-ray and ultraviolet (XUV) as well as the acceleration of stellar winds that have a wide range of effects on planets and their atmospheres (Johnstone et al. 2021). Murray-Clay et al. (2009) suggested that high-energy radiation from X-ray and XUV radiation is absorbed in the upper atmosphere of planets, which carries dissociation, ionization, and heating. This process enhances and drives atmospheric loss, including rapid

hydrodynamic losses if the star's activity is high enough.

Yang & Johns-Krull (2011) measured the magnetic fields in T Tauri stars in the Orion Nebula Cluster. These low-mass variable stars often display many spectral peculiarities, such as excess in the emission from ultraviolet through infrared wavelengths. They found that stars at birth have very strong magnetic fields and high XUV luminosities. However, these strong magnetic fields and XUV decay rapidly during the first few million years. Vidotto et al. (2014) investigated large-scale surface magnetic fields of low-mass stars in the pre-main sequence to the main sequence to examine the relationship of their ages ($1\mathrm{Myr} \lesssim \mathrm{t} \lesssim 10~\mathrm{Gyr}$), rotation, and X-ray emissions. At later ages, stars' spin-down causes significant decay in magnetic fields and high energy emission.

Claire et al. (2012) Investigate solar flux changes to understand the planetary atmosphere's evolution because it affects the atmospheric escape and chemistry. They found a rapid decay of XUV emission at shorter wavelengths, which causes the shape of the XUV spectrum to evolve. A star's (F, G, K, and M dwarfs) X-ray, EUV, and Ly-α evolution are determined by its mass, age, and initial rotation rate. Solar-mass stars, at all ages, are more X-ray luminous than lower-mass stars, and stars that are born as rapid rotators remain highly active longer than stars that are born as slow rotators (Johnstone et al. 2021).

As we can see, stellar activity is intrinsically correlated with the planet's atmosphere. However, different parameters could also contribute to characterizing the exoplanetary atmosphere. We will discuss those in Section **??**.

5.2 Detection and non-detection of Hα

In the literature, we have discovered various elements since the first chemical signature detection in an exoplanetary atmosphere. Then, following Section 1.3.2, we will detail the Hα detection considering additional parameters for each detection or non-detections.

Winn et al. (2004) reported a no detection of Hα absorption signature in HD-209458b exosphere, orbiting an early G-type star (or late F-type star) every 3.5 days. Jensen et al. (2012) made the first Hα detection in the HD-189733b atmosphere, orbiting a K1.5V spectral type star every 2.2 days. In addition, Jensen et al. (2012) also reported a no-detection of Hα signatures in the HD-149026b, HD-209458b, and HD-147506b atmosphere. HD-149026b is orbiting a G0 star every 2.9 days, while HD-209458b and HD-147506b are orbiting an F8 star every 3.5 days and 5.6 days, respectively. Yan & Henning (2018); Wyttenbach et al. (2020) reported Hα absorption signature in KELT-9b atmosphere orbiting an early A-type (or late B-type star) star every 1.48 days. Jensen et al. (2018) reported Hα detection in the WASP-12b, a planet orbiting its G0V-type star every 1.1 days. In 2023, a potential detection of Hα was reported in the lowest-density Saturn-mass exoplanet (HAT-P-67b) in orbit (4.8 days) of an F-type star. In 2019, a detection of Hα signature was reported in the MASCARA-2b/KELT-20b exoplanet atmosphere (Casasayas-Barris et al. 2019). This planet is orbiting an A-type star every 3.47 days. Carleo et al. (2021) reported a no detection for GJ-9827b exoplanet orbiting a K-type stars. Casasayas-Barris et al. (2022) also reported no detection in the planetary atmosphere of MASCARA-1b orbiting a A-type star.

Table 5.1 summarizes Hα absorption detections and non-detections for exo-

planets orbiting stars of different spectral types. We will discuss each parameter in the table in Section 5.4.

Planet	R (M_{Jup})	T_{eq} (K)	Period (days)	Spectral type	Age (Gyr)	Detect.
HD-189733b	1.119 ± 0.038	1209 ± 11	2.2	K1.5V	$6.80^{+5.20}_{-4.40}$	Yes
KELT-9b	$1.891^{+0.061}_{-0.053}$	4050 ± 180	1.48	late B/early A	0.3	Yes
MASCARA-2b	1.83 ± 0.07	2260 ± 50	$3.474119^{+0.000005}_{-0.000006}$	A2	$0.200^{+0.100}_{-0.050}$	Yes
WASP-12b	1.465 ± 0.079	2592.6 ± 57.2	$1.09142245\pm3\times10^{-7}$	GOV	$2.00^{+0.70}_{-2.00}$	Yes
HD-209458b	1.42 ± 0.10	1449 ± 12	3.5	Early G /lateF	$3.10^{+0.80}_{-0.70}$	No
HD-149026b	$0.610^{+0.099}_{-0.072}$	1626^{+69}_{-37}	2.9	G0	2.22 ± 0.44	No
HD-209458b	1.36	1450	3.5	F8	$3.10^{+0.80}_{-0.70}$	No
HD-147506b	1.1	1700	5.6	F8	1.44 ± 0.47	No
HAT-P-67b	$2.085^{+0.096}_{-0.07}$	1903 ± 25	4.8	F	$1.24^{+0.27}_{-0.22}$	cand.
GJ-9827b	$0.128^{+0.008}_{-0.006}$	1035.01 ± 29.07	1.208974 ± 0.000001	K7V	5.465 ± 4.058	No
MASCARA-1b	3.7 ± 0.9	$2570+50-30$	2.148780 ± 0.000008	A8	1.0 ± 0.2	No
TOI-1288b	0.467 ± 0.008	1266 ± 27	2.7	GV	$12.1^{+1.4}_{-3.1}$	No

Table 5.1: Hα absorption detections and no-detections. This table displays an exoplanet's main parameters. Where the Radius and equilibrium temperature (T_{Eq}) of each of them has been taken as follows: HD-189733 (Addison et al. 2019), HD-149026b (Southworth 2010), HD-209458b (Sing et al. 2016), HD-147506b (Salz et al. 2015), KELT-9b (Gaudi et al. 2017), WASP-12b (Chakrabarty & Sengupta 2019), HAT-P-67b (Zhou et al. 2017), TOI-1288b (Knudstrup et al. 2023), GJ-9827b (Passegger et al. 2024), MASCARA-2b (Talens et al. 2018) and MASCARA-1b (Talens et al. 2017). The corresponding ages of listed planets were taken as follows: HD-209458b (Bonomo et al. 2017), HD-189733b (Addison et al. 2019), HD-149026b (Ment et al. 2018), HD-147506b (Ment et al. 2018), KELT-9b (Gaudi et al. 2017), WASP-12b (Bonomo et al. 2017), HAT-P-67b (Zhou et al. 2017), GJ-9827b (Passegger et al. 2024), MASCARA-2b (Talens et al. 2018) and MASCARA-1b (Talens et al. 2017)

5.3 Non-detection of Hα on TOI-1288b extended atmosphere

The location of TOI-1288b in the Neptune desert gave us the first sign that this planet could be experiencing a planetary escape from its extended atmosphere. However, we did not detect any Hα absorption signature, as shown in Figure 5.1. In the figure, we over-plot Vidotto's model to our transmission spectrum. The model shows a small absorption signature of Hα that was not detected in our data.
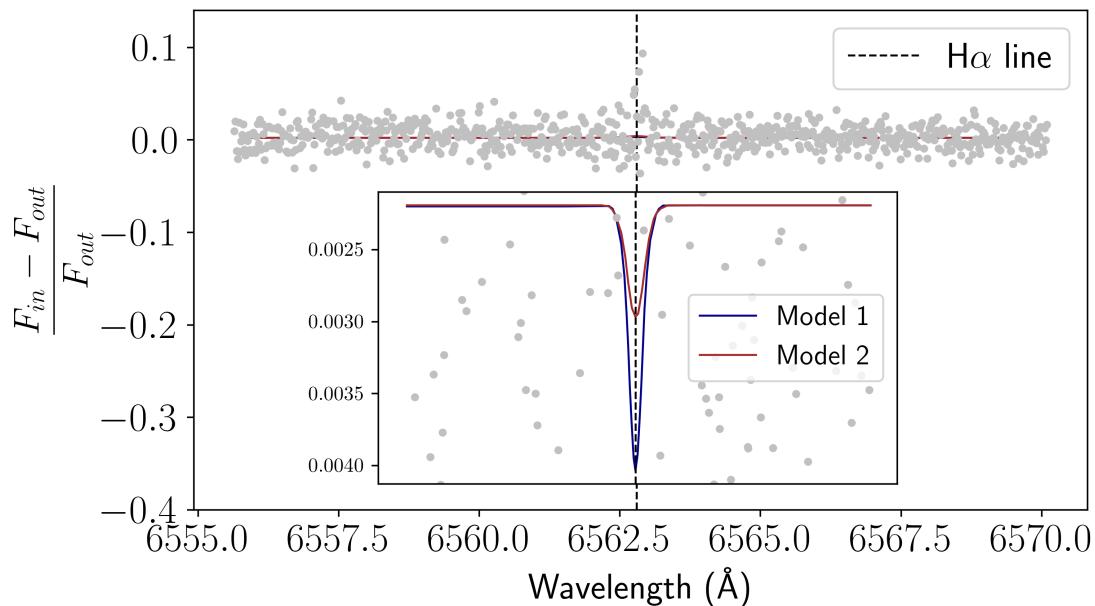

Figure 5.1: Model and transmission spectrum of TOI-1288b.

Sections 5.1 and 5.2 give an overview of the parameters related to the star-planet system. Since stellar magnetic activity shapes the exoplanet's atmosphere, bringing X-rays and XUV radiation onto the planet, where the X-rays and XUV radiation are intrinsically related to the mass and age of the host star. TOI-

1288b's host star is a $12.1^{+1.4}_{-3.1}$ G-type star, and due to its age, we can suggest that this star has weak X-ray and XUV radiation reaching the TOI-1288b extended atmosphere. Therefore, this weak stellar radiation cannot excite hydrogen atoms into Hα transitions (n=2). On the other hand, this non-detection could be because the planet already lost its atmosphere during the early ages of the star, which means that the strong radiation of a young star on the planet's atmosphere caused it to lose its atmosphere a long time ago.

To sum up, those are the main explanations for the no-detection of Hα absorption in the TOI-1288b. However, there are other parameters that we can address to understand it (See Section **??**).

5.4 Different parameters related to the Hα detection

Addressing different parameters related to Hα may offer insight into any trends in atmospheric escape. Table 5.1 shows some properties of detection and non-detection of Hα. The age column in the table shows that most of the stars listed are billion-year-old stars going from A to K spectral type. The Hα detection corresponds to B, A, G, and K spectral types. However, these characteristics do not seem to follow a trend because we have detections with similar spectral types and ages. Equilibrium temperature (T_{eq}) is another column to look at, as we see planets with Hα detection have high T_{eq}, but also we have high T_{eq} in the no detections. From the Radius and Period columns, we have similar radius and period for detection and not detection. Therefore, it seems that there is no clear trend to follow.

Through the analysis of the table, we can notice that the TOI-1288 system has

almost the same parameters as the rest of the planets listed in the table. However, if we look at the age of TOI-1288b's host star, it appears in the table as the oldest star compared to the rest.

Chapter 6

Conclusion and Future Expectations

6.1 A Summary of non-detection of Hα in TOI-1288b extended atmosphere

In this thesis, we search for the Hα absorption line in the extended atmosphere of TOI-1288b, a hot super-Neptune located in the Neptune desert orbiting every $\sim$ 2.7 days a late G-type star. We took a one-transit observation of TOI-1288b because its location in the Neptune desert makes it a perfect candidate to search for atmospheric escape, and it is known planets close to their host star are experiencing high rates of high-energy radiation. And if this constant radiation is high enough, it could cause atmospheric escape and eventual mass loss on the planet. Therefore, the mechanism of losing mass due to atmospheric escape is an important feature of formation and evolution studies.

We used Rossiter-McLaughlin (RM) observations to obtain the TOI-1288b transmission spectrum. Observation data were taken using a high-resolution ground-based spectrograph (HARPS-N) in the visible spectrum range (3780 - 6910 Å). From the planet transit duration (2.37 hours), we obtained 9 exposures to construct the in-transit and out-of-transit and, finally, the transmission spectrum. In addition, we developed the propagation error theory on the data to measure the Hα upper limit (3σ), which results comparable to Jensen et al. (2012).

As a result of a flat transmission spectrum and not Hα absorption signature, we compared our transmission spectrum result to Vidotto's model 5.1). The developed Hα absorption profile model is based on stellar and planetary mass, radius, temperature, and the stellar XUV radiation. Surprisingly, the model predicted a Hα absorption signature. However, we argue that the reason that it is not detected in our transmission spectrum is because it is a weak signature.

6.2 Recommendations and future work

Planetary atmospheric escape plays an important role in our understanding of planetary evolution. The first discovered planet orbiting a solar-type star was a starting breaking point in this field. So, the detection of Hα as well as Lyα signatures becomes a standard indicator in planets that are experiencing atmospheric escape. Therefore, determining both signatures or using one of them to find the other allows astronomers to corroborate their findings. This has been done for HD-189773 (Vidal-Madjar et al. 2003; Salz et al. 2018), 55-Cnc-e (Ehrenreich et al. 2012; Zhang et al. 2021), GJ-436b (Villarreal D'Angelo et al. 2021) and GJ-9827b (Carleo et al. 2021).

Another corroboration technique should be to have higher signal-to-noise in the observations to see a weak Hα signature in the transmission spectrum. To do that, we need a bigger telescope to collect enough light from the observations and obtain a higger signal-to-noise relationship in the data. In addition, to improve our observations, it is important to include multiple transits for the observed target because that can allow us to have enough data and perform different mathematical analyses such as the Empirical Monte Carlo Method (EMC).

Modeling Hα or Lα profiles requires specific parameters. One of the most

important and difficult to estimate is the XUV radiation. The effects of this type of radiation take place at different heights of the planetary atmosphere. While EUV photons mainly ionize the atoms in the upper atmosphere, X-rays penetrate deeper into the atmosphere (Sanz-Forcada et al. 2011). Therefore, it is important to estimate an accurate value of this parameter in order to obtain more realistic models.

Target selection also plays an important role when we are doing research. Some parameters can be considered. For example, we can search for planets with high equilibrium temperatures closer to their host stars. We can also consider the type of star these planets are orbiting and the age and stellar activity of the host stars. Those are some ideas if a researcher is looking to make a full analysis of any exoplanetary system.

Finally, exoplanets' atmospheres are not just possess Hα and/or Lα signatures. Exoplanetary atmospheres are also rich in other species, such as sodium (Na), potassium (K), magnesium (Mg), etc., that have been reported in the literature. For example, a Na detection in HD-189733b (Redfield et al. 2008), Mg in HD-209458 b (Vidal-Madjar et al. 2013) and K in WASP-17b Sedaghati et al. (2016). Therefore, to follow these findings in future work, we must continue looking at the TOI-1288b atmosphere. We did a rough survey of our data and found Na, K, and Mg in the TOI-1288 stellar spectra. So, as a next step, we will be moving to search for signatures of those lines in the planetary atmosphere of TOI-1288b.

Bibliography

Addison, B., et al. 2019, PASP, 131, 115003

Bakos, G. Á., et al. 2007, ApJ, 670, 826

Baraffe, I., Chabrier, G., Barman, T. S., Selsis, F., Allard, F., & Hauschildt, P. H. 2005, A&A, 436, L47

Barstow, J. K., Aigrain, S., Irwin, P. G. J., & Sing, D. K. 2017, ApJ, 834, 50

Bello-Arufe, A., et al. 2023, AJ, 166, 69

Bennett, K. 2022, Master's thesis, Wesleyan University, Connecticut

Bevington, P. R., & Robinson, D. K. 2003, Data reduction and error analysis for the physical sciences

Bonomo, A. S., et al. 2017, A&A, 602, A107

Brown, T. M. 2001, ApJ, 553, 1006

Bruno, G. 1980, in The Quest for Extraterrestrial Life, ed. D. Goldsmith, 5

Carleo, I., et al. 2021, AJ, 161, 136

Casasayas-Barris, N., et al. 2022, A&A, 664, A121

—. 2019, A&A, 628, A9

Chakrabarty, A., & Sengupta, S. 2019, AJ, 158, 39

Charbonneau, D., Brown, T. M., Latham, D. W., & Mayor, M. 2000, ApJ, 529, L45

Charbonneau, D., Brown, T. M., Noyes, R. W., & Gilliland, R. L. 2002, ApJ, 568, 377

Christie, D., Arras, P., & Li, Z.-Y. 2014, in Exploring the Formation and Evolution of Planetary Systems, ed. M. Booth, B. C. Matthews, & J. R. Graham, Vol. 299, 281–282

Chromey, F. R. 2016, To Measure the Sky

Claire, M. W., Sheets, J., Cohen, M., Ribas, I., Meadows, V. S., & Catling, D. C. 2012, ApJ, 757, 95

Cosentino, R., et al. 2012, in Society of Photo-Optical Instrumentation Engineers (SPIE) Conference Series, Vol. 8446, Ground-based and Airborne Instrumentation for Astronomy IV, ed. I. S. McLean, S. K. Ramsay, & H. Takami, 84461V

Deeg, H. J., & Alonso, R. 2018, in Handbook of Exoplanets, ed. H. J. Deeg & J. A. Belmonte, 117

Ehrenreich, D., et al. 2012, A&A, 547, A18

Fortney, J. J., Dawson, R. I., & Komacek, T. D. 2021, Journal of Geophysical Research (Planets), 126, e06629

Gaudi, B. S., et al. 2017, Nature, 546, 514

Guerrero, N. M., et al. 2021, ApJS, 254, 39

Heller, R. 2019, A&A, 623, A137

Henry, G. W., Marcy, G. W., Butler, R. P., & Vogt, S. S. 2000, ApJ, 529, L41

Hoeijmakers, H. J., et al. 2019, A&A, 627, A165

Howe, A. R., Adams, F. C., & Meyer, M. R. 2020, ApJ, 894, 130

Huang, C., Arras, P., Christie, D., & Li, Z.-Y. 2017, ApJ, 851, 150

Hubbard, W. B., Hattori, M. F., Burrows, A., & Hubeny, I. 2007, ApJ, 658, L59

Jenkins, J. M., et al. 2016, in Society of Photo-Optical Instrumentation Engineers (SPIE) Conference Series, Vol. 9913, Software and Cyberinfrastructure for Astronomy IV, ed. G. Chiozzi & J. C. Guzman, 99133E

Jensen, A. G., Cauley, P. W., Redfield, S., Cochran, W. D., & Endl, M. 2018, AJ, 156, 154

Jensen, A. G., Redfield, S., Endl, M., Cochran, W. D., Koesterke, L., & Barman, T. 2012, ApJ, 751, 86

Jensen, E. 2013, Tapir: A web interface for transit/eclipse observability, Astrophysics Source Code Library, record ascl:1306.007

Johnstone, C. P., Bartel, M., & Güdel, M. 2021, A&A, 649, A96

Kennedy, G. M., & Kenyon, S. J. 2008, ApJ, 673, 502

Kipping, D. M. 2013, MNRAS, 435, 2152

Knudstrup, E., et al. 2023, MNRAS, 519, 5637

Koskinen, T. T., Lavvas, P., Huang, C., Bergsten, G., Fernandes, R. B., & Young, M. E. 2022, ApJ, 929, 52

Kreidberg, L. 2015, PASP, 127, 1161

Kubyshkina, D. 2024, arXiv e-prints, arXiv:2402.13931

Magliano, C., et al. 2023, MNRAS, 519, 1562

Mayor, M., & Queloz, D. 1995, Nature, 378, 355

Mayorga, L. C., et al. 2021, , 2, 140

Mazeh, T., Holczer, T., & Faigler, S. 2016, A&A, 589, A75

McCann, J., Murray-Clay, R. A., Kratter, K., & Krumholz, M. R. 2019, ApJ, 873, 89

Ment, K., Fischer, D. A., Bakos, G., Howard, A. W., & Isaacson, H. 2018, AJ, 156, 213

Menzel, M., et al. 2023, PASP, 135, 058002

Murray-Clay, R. A., Chiang, E. I., & Murray, N. 2009, ApJ, 693, 23

Nardetto, N., et al. 2023, A&A, 671, A14

Owen, J. E., & Adams, F. C. 2019, MNRAS, 490, 15

Owen, J. E., & Lai, D. 2018, MNRAS, 479, 5012

Paice, J. A., & J. C Watkins, J. 2022, arXiv e-prints, arXiv:2203.17075

Passegger, V. M., et al. 2024, A&A, 684, A22

Piskunov, N. E., & Valenti, J. A. 2002, A&A, 385, 1095

Rao, S., et al. 2021, A&A, 651, A50

Rauer, H., Bockelée-Morvan, D., Coustenis, A., Guillot, T., & Schneider, J. 2000, A&A, 355, 573

Redfield, S., Endl, M., Cochran, W. D., & Koesterke, L. 2008, ApJ, 673, L87

Ricker, G. R., et al. 2015, Journal of Astronomical Telescopes, Instruments, and Systems, 1, 014003

Salz, M., et al. 2018, A&A, 620, A97

Salz, M., Schneider, P. C., Czesla, S., & Schmitt, J. H. M. M. 2015, A&A, 576, A42

Sanz-Forcada, J., Micela, G., Ribas, I., Pollock, A. M. T., Eiroa, C., Velasco, A., Solano, E., & García-Álvarez, D. 2011, A&A, 532, A6

Sato, B., et al. 2005, ApJ, 633, 465

Schneider, J. 1994, Ap&SS, 212, 321

Seager, S., & Deming, D. 2010, ARA&A, 48, 631

Seager, S., & Sasselov, D. D. 2000, ApJ, 537, 916

Sedaghati, E., et al. 2016, A&A, 596, A47

Sing, D. K., et al. 2016, Nature, 529, 59

Smette, A. 2020, in Ground-Based Thermal Infrared Astronomy - Past, Present and Future, 46

Southworth, J. 2010, MNRAS, 408, 1689

Szabó, G. M., & Kálmán, S. 2019, MNRAS, 485, L116

Szabó, G. M., & Kiss, L. L. 2011, ApJ, 727, L44

Talens, G. J. J., et al. 2017, A&A, 606, A73

—. 2018, A&A, 612, A57

Torres, G., Winn, J. N., & Holman, M. J. 2008, ApJ, 677, 1324

Triaud, A. H. M. J. 2018, in Handbook of Exoplanets, ed. H. J. Deeg & J. A. Belmonte, 2

Vidal-Madjar, A., et al. 2013, A&A, 560, A54

Vidal-Madjar, A., Lecavelier des Etangs, A., Désert, J. M., Ballester, G. E., Ferlet, R., Hébrard, G., & Mayor, M. 2003, Nature, 422, 143

Vidotto, A. A., & Cleary, A. 2020, MNRAS, 494, 2417

Vidotto, A. A., et al. 2014, MNRAS, 441, 2361

Villarreal D'Angelo, C., Vidotto, A. A., Esquivel, A., Hazra, G., & Youngblood, A. 2021, MNRAS, 501, 4383

Winn, J. N., Suto, Y., Turner, E. L., Narita, N., Frye, B. L., Aoki, W., Sato, B., & Yamada, T. 2004, PASJ, 56, 655

Wolszczan, A., & Frail, D. A. 1992, Nature, 355, 145

Wright, J. T., & Kanodia, S. 2020, , 1, 38

Wyttenbach, A., et al. 2020, A&A, 638, A87

Yan, F., & Henning, T. 2018, Nature Astronomy, 2, 714

Yang, H., & Johns-Krull, C. M. 2011, ApJ, 729, 83

Zhang, M., Knutson, H. A., Wang, L., Dai, F., Oklopcic, A., & Hu, R. 2021, AJ, 161, 181

Zhou, G., et al. 2017, AJ, 153, 211